Geometric manipulation of ensembles of atoms on an atom chip for quantum computation

Yi-Cong Zheng and Todd A. Brun

Phys. Rev. A **86**, 032323 — Published 18 September 2012

DOI: 10.1103/PhysRevA.86.032323

Geometric Manipulation of Ensembles of Atoms on Atom Chip for Quantum Computation

Yi-Cong Zheng* and Todd A. Brun†
Department of Electrical Engineering,
Center for Quantum Information Science & Technology,
University of Southern California,
Los Angeles, California, 90089

We propose a feasible scheme to achieve quantum computation based on geometric manipulation of ensembles of atoms, and analyze it for neutral rubidium atoms magnetically trapped in planoconcave microcavities on an atom chip. The geometric operations are accomplished by optical excitation of a single atom into a Rydberg state in a constant electric field. Strong dipole-dipole interactions and incident lasers drive the dark state of the atom ensembles to undergo cyclic evolutions that realize a universal set of quantum gates. Such geometric manipulation turns out naturally to protect the qubits from the errors induced by non-uniform laser illumination as well as cavity loss. The gate performance and decoherence processes are assessed by numerical simulation.

PACS numbers: 03.65.Vf, 03.67.Lx, 42.50.Pq, 32.80.Ee

I. INTRODUCTION

Quantum information processing (QIP) holds out the possibility to run algorithms and protocols superior to those of its classical counterpart [1, 2]. In recent decades, numerous candidates for physical implementation of quantum information processors have been proposed [3]. Because of long coherence times and exceptional controllability, quantum optical and atomic systems such as trapped ions [4, 5], neutral atoms [6, 7], and cavity QED [8, 9], have taken a leading role in implementing quantum logic. Photons are remarkably robust candidates for qubits, and are easy to transport long distances; however, as we know, they interact only weakly with each other, which makes the realization of quantum gates based on photons difficult. For instance, in linear optical quantum computation (LOQC) [10], extra measurements are required, and the resulting gates succeed only probabilistically. On the other hand, ensembles of trapped atoms or molecules may serve as convenient and robust quantum memories for photons. They can act as an interface with flying qubits, and store and retrieve single photons, for example by electromagnetically induced transparency (EIT) [11, 12], which can preserve coherence of quantum states for up to several hundreds of milliseconds [13].

One might therefore hope to use controlled interactions in the ensemble of atoms, once the flying qubits are stored, to realize universal quantum logic gates in a deterministic and scalable way. Several promising schemes for such operations, based on combining EIT with Rydberg atoms, were proposed in Ref. [14, 15], exciting atoms with lasers to high-lying Rydberg states and exploiting the long-range dipole-dipole interaction between Rydberg states. Recent theoretical proposals include single-step, high-fidelity entanglement of a mesoscopic number of atoms [16], and quantum simulation of both coherent dynamics and dissipative evolution processes for many body systems [17]. Remarkably, the building blocks of such proposals have been demonstrated experimentally by several groups [18, 19]. In Ref. [20], an effective strong dipole-dipole blockade effect is achieved by coupling to microwave coplanar waveguide resonators to realize quantum logic on ensembles of molecules. However, dynamical control of such an ensemble is difficult due to the inhomogeneous coupling between laser and atoms, and it suffers from control noise as well. In addition, proposals for geometric manipulation of ions [21] and neutral atoms [22] have been made for their natural robustness against certain control errors. However, for the single ion or atom in these proposals it is very difficult to transfer the photon signal to the matter states, and it needs an extremely good cavity to realize a high fidelity two-qubit quantum gate due to the small coupling efficiency.

To overcome the problems mentioned above, we put forward here an alternative, scalable approach to realize universal quantum gates based solely on laser-controlled geometric manipulation of neutral atomic clouds trapped on the surface of atom chips. The paper is organized as follows. In section II, we introduce the basic model of the atom/cavity system. Then, we show how to construct the Hamiltonian of the system, and how to adiabatically manipulate the evolution to implement three quantum gates geometrically: the phase gate, the y-rotation gate, and the controlled phase gate. These constructions are given in sections IIIA, IIIB, and IIIC, respectively. Numerical analysis of their performance is also given in these three sections. These three gates form a universal set of quantum logic gates. In section IV, we show how to perform qubit measurements on this system. Finally, both analysis and numerical study of decoherence and its effect

*Electronic address: yicongzh@usc.edu
†Electronic address: tbrun@usc.edu

on our system are given in section V, and we conclude in section VI. In an Appendix to the paper, we discuss how to choose suitable Rydberg states for this scheme, in rubidium or other alkali atoms.

II. MODEL

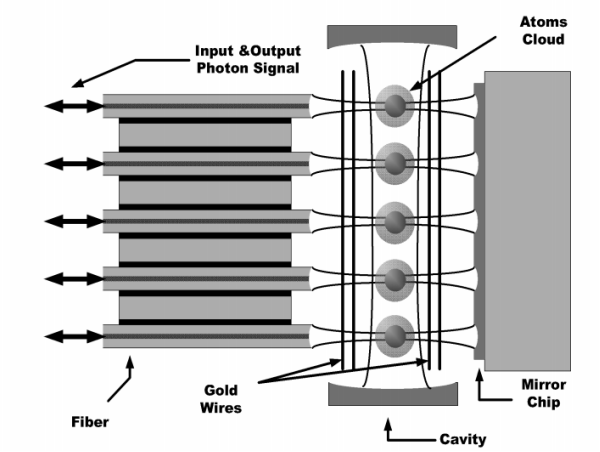

FIG. 1: Schematic of trapped ensembles of atoms in magnetic atom traps inside plano-concave optical microcavities (horizontal). Each atomic cloud is a qubit, and forms a processing cell. Different qubits couple to each other mediated by the photonic modes of another Fabry-Perot cavity (vertical).

Atom chips supply a good platform for precise control and manipulation of neutral atoms [23, 24]. We will show that an atom chip with integrated Fabry-Perot (FP) microcavities can realize a universal set of all-optical universal quantum gates for atomic ensemble qubits.

Consider several plano-concave Fabry-Perot (FP) microcavities resonators [25] integrated on the atom chip, which are parallel to each other. Another large FP cavity is integrated so that its mode is perpendicular to all the plano-concave cavities. A schematic diagram is shown in Fig. 1. A plano-concave resonator consists of an isotropically etched dip in a silicon surface, and the cleaved tip of a single-mode fiber [26] serves as the input-output channel. Atomic ensembles are placed in the region of highest field strength of the cavity modes, leading to higher values of the coupling g, and a Q value over 10^6. The perpendicular FP cavity modes serve as a data bus to couple different qubits.

The atomic clouds must be confined in traps inside the cavities. We can introduce magnetic fields produced by current-carrying wires on the surface and coupled to the magnetic dipole of the atoms. The small scale of the structure produces strong magnetic field gradients, which make tight traps for magnetic atoms. Atoms in a weak-field-seeking state will be attracted and held in this region. The hyperfine states $|F = 2, m_F = 1\rangle$ and $|F = 1, m_F = -1\rangle$ of $5S_{1/2}$ of ^{87}Rb are ideal weak-field-seeking states that can be trapped by a static magnetic

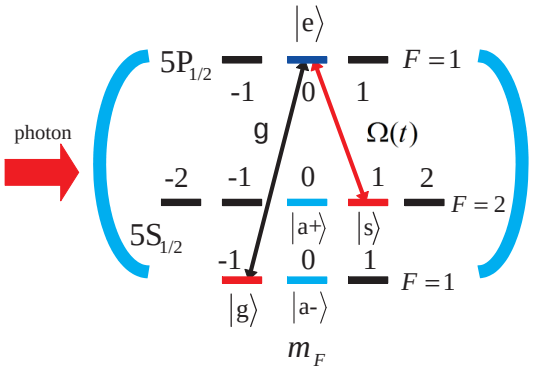

FIG. 2: (Color online.) Storage of a single photon qubit. The level scheme of a single ^{87}Rb atom is shown. The input qubit is encoded as $|0\rangle$ if there is no photon in the input mode, and $|1\rangle$ if there is a photon in the input mode. Here, we use the hyperfine levels of manifold $5S_{1/2}$: clock states $|g\rangle = |F = 1, m_F = -1\rangle$ and $|s\rangle = |F = 2, m_F = 1\rangle$; $|a_-\rangle = |F = 1, m_F = 0\rangle$ and $|a_+\rangle = |F = 2, m_F = 0\rangle$ are used as ancillary states. A state of manifold $5P_{1/2}$ serves as an intermediate state $|e\rangle$ ($|F = 1, m_F = 0\rangle$). The storage process mapping single photon signals into collective excited atomic states of $|s\rangle$ can be accomplished by adiabatically turning on the classical laser field $\Omega(t)$ to a value much larger than the coupling constant g when the photon arrives. The reverse process can be used to read out the photon.

potential [23]. In addition, these two states have opposite Landé factors, so that they experience identical magnetic potentials. Thus, the decoherence of an arbitrary superposition of these two states due to current intensity fluctuations is strongly inhibited [27]. Coherent oscillations between these states have been observed with decoherence times as long as $\tau_c = 2.8 \pm 1.6$s [28]. So it is natural to consider these two states of ^{87}Rb for quantum information processing.

The state of the ^{87}Rb atom cloud can be initialized by inputting a single photon qubit to the plano-concave cavity through the fiber, as shown in Fig. 2. The state $|0\rangle_{\rm ph}$ corresponds to no photons in the input channel, and the state $|1\rangle_{\rm ph}$ corresponds to one photon. An arbitrary qubit state can be represented as $\alpha|0\rangle_{\rm ph} + \beta|1\rangle_{\rm ph}$. In general, the state of n input channels is an entangled state in a Hilbert space of dimension 2^n.

An ensemble of N identical multi-state atoms is trapped in each cell. Using well-developed techniques, all atoms can be initially prepared and trapped in a specific sub-level (hyperfine level $|g_i\rangle$, $i = 1, 2, 3, ..., N$) of the internal atomic ground space manifold [14]. Relevant states of each atom include the other clock state $|s_i\rangle$, two ancillary states $|a_{-i}\rangle, |a_{+i}\rangle$ (which are chosen not be affected by the magnetic potential), and an intermediate state $|e_i\rangle$. (As mentioned earlier, $|s_i\rangle$ has a long coherence time.) We also assume the atomic density is not too high, so that interaction between atoms can be safely neglected. Atoms are manipulated by illuminating the entire ensemble, to excite all atoms with equal prob-

ability, so only symmetric collective states are involved in this process [14]. For loading quantum information into the ensembles, we consider only three states: $|e_i\rangle$, $|s_i\rangle$ and $|g_i\rangle$, where $|e_i\rangle$ and $|g_i\rangle$ are coupled to the cavity mode of the plano-concave cavity, while $|e_i\rangle$ and $|s_i\rangle$ are coupled by a classical field. Initially, all the atoms are in their ground states:

$$|\mathbf{g}\rangle = |\mathbf{g}^N\rangle = |g_1\rangle ... |g_N\rangle.$$

We define operators

$$\hat{\mathcal{S}} = \frac{1}{\sqrt{N}} \sum_i |g_i\rangle\langle s_i|,$$

$$\hat{\mathcal{E}} = \frac{1}{\sqrt{N}} \sum_i |g_i\rangle\langle e_i|,$$

$$\hat{\mathcal{A}}_{\pm} = \frac{1}{\sqrt{N}} \sum_i |g_i\rangle\langle a_{\pm i}|.$$

The storage state with excitation n is

$$|\mathbf{s}^n\rangle \equiv |\mathbf{g}^{N-n}, \mathbf{s}^n\rangle = \sqrt{\frac{(N-n)!N^n}{N!n!}} (\hat{\mathcal{S}}^\dagger)^n |\mathbf{g}\rangle.$$

For the case when $n = 1$, this is

$$\begin{aligned} |\mathbf{s}\rangle \;=\; & \frac{1}{\sqrt{N}} \big(|s_1, g_2, g_3 ... g_N\rangle + |g_1, s_2, g_3 ... g_N\rangle \\ & + \cdots + |g_1, g_2, g_3 ... s_N\rangle \big). \end{aligned}$$

The commutation relation of $\hat{\mathcal{S}}$ and $\hat{\mathcal{S}}^\dagger$ is

$$[\hat{\mathcal{S}}, \hat{\mathcal{S}}^\dagger] = 1 - \frac{2n}{N}.$$

For a sufficiently small number of excitations ($n \ll N$), these two operators can be approximated by bosonic annihilation and creation operators of quasiparticles corresponding to $|s\rangle$. Operators $\hat{\mathcal{E}}$ and $\hat{\mathcal{E}}^\dagger$, and $\hat{\mathcal{A}}_{\pm}$ and $\hat{\mathcal{A}}_{\pm}^\dagger$ have the same properties.

As shown in Ref. [29] and Ref. [30], when the photon arrives in the cavity, one can adiabatically turn on the classical field coupling the states $|e\rangle$ and $|s\rangle$, until the Rabi frequency Ω is much larger than the cavity-atom coupling constant g. The state of the photon mode is stored in the ensemble of atoms in the cavity in the form $|n\rangle_{\rm ph} \to |\mathbf{s}^n\rangle$, where $|n\rangle_{\rm ph}$ represents the n-photon Fock state. This process is reversible: one can retrieve the photon from the ensemble of atoms. So, an arbitrary input state $\alpha|0\rangle_{\rm ph} + \beta|1\rangle_{\rm ph}$ can be mapped into the state $\alpha|\mathbf{g}\rangle + \beta|\mathbf{s}\rangle$ with high fidelity [29]. We denote $|0\rangle_L = |\mathbf{g}\rangle$ and $|1\rangle_L = |\mathbf{s}\rangle$ for the logical representation of a qubit in each cloud of atoms.

III. A UNIVERSAL SET OF GEOMETRIC GATES

We now discuss how to geometrically implement quantum computation (holonomic quantum computation [31]) in our system. The first step is to construct a Hamiltonian that has an eigenspace with eigenvalue 0 to avoid dynamic phase during the cyclic evolution. This eigenspace can either be nondegenerate, which would introduce simple Abelian phase factors (Berry phases) [32], or degenerate, which could cause general non-Abelian operations [33]. It is well known that single-qubit operations, together with a nontrivial two-bit gate, make a universal set of quantum logic gates for quantum computation [34]. By constructing an appropriate set of looped paths in the parameter space we can obtain an arbitrary unitary transformation in the computational space.

We choose for our universal set of gates

$$R_z^{(i)}(\phi_1) = \exp\Big(i\phi_1 |1_i\rangle_{LL}\langle 1_i| \Big),$$

$$R_y^{(i)}(\phi_2) = \exp\Big(i\phi_2 \sigma_i^y \Big),$$

$$U^{(jk)}(\phi_3) = \exp\Big(i\phi_3 |1_j 0_k\rangle_{LL}\langle 1_j 0_k| \Big).$$

The states $|0_i\rangle_L$ and $|1_i\rangle_L$ are the computational basis states for qubit i, and σ_i^y is the Pauli operator in the y direction for the ith qubit. If we can implement these gates with arbitrary ϕ_1, ϕ_2, ϕ_3, we can implement all unitary transformations [34]. The three operators correspond to a rotation in the z direction, a rotation in the y direction, and a conditional phase rotation when qubits j and k are in the state $|10\rangle_L$. In this section, we show how to holonomically realize these three gates.

A. One Qubit Phase Gate

We first consider how to perform a simple one qubit phase gate: $|1\rangle_L \to e^{i\phi_1}|1\rangle_L$. To simplify the model, we only consider the energy levels we are interested in. The total pulse sequence and resonant coupling diagram is shown in Fig. 3. The Hamiltonian of this system, in the interaction picture and rotating wave approximation, is

$$\begin{aligned} H_1(t) = & \sum_i \Omega_1^i(t) \big(\sigma_{se}^{(i)} + \text{H.c} \big) \\ & + \sum_i \Omega_a^i(t) \big(\sigma_{a+e}^{(i)} + \text{H.c} \big), \end{aligned} \tag{1}$$

where the $\sigma_{jk}^{(i)} = |j_i\rangle\langle k_i|$ are transition operators from state $|k\rangle$ to $|j\rangle$ for atom i, and $\hbar = 1$. Here, the two lasers are assumed to be phase matched, and their Rabi

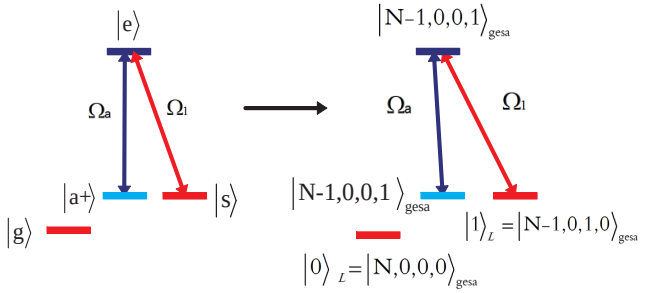

FIG. 3: (Color Online.) Left: Level structure and laser coupling diagram for a single atom. Right: The equivalent coupling diagram for an ensemble of atoms in second quantized representation.

frequencies are real numbers. For simplicity, assuming the laser beams illuminate each atom with same intensity, we can rewrite the Hamiltonian in the second quantized representation:

$$\begin{aligned} H_1(t) =& \Omega_1(t)\hat{\mathcal{E}}^\dagger\hat{\mathcal{S}} + \Omega_1^*(t)\hat{\mathcal{S}}^\dagger\hat{\mathcal{E}} \\ &+ \Omega_a(t)\hat{\mathcal{E}}^\dagger\hat{\mathcal{A}}_+ + \Omega_a^*(t)\hat{\mathcal{A}}_+^\dagger\hat{\mathcal{E}}, \end{aligned} \tag{2}$$

and set $\Omega_1 = \Omega\sin\theta$ and $\Omega_a = -\Omega\cos\theta e^{i\varphi}$. The parameters θ and φ are functions of time, and the absolute magnitude Ω is a constant that must be large enough to satisfy the adiabatic condition. $\hat{\mathcal{E}}, \hat{\mathcal{S}}, \hat{\mathcal{A}}_+$ are bosonic operators defined in last section corresponding to the single atom states $|e\rangle, |s\rangle, |a_+\rangle$, respectively.

We can treat the system as three coupled harmonic oscillators. We are only interested in singly excited states; the Hamiltonian discussed above is closed in that basis, which for simplicity we represent as $\{|\mathbf{e}\rangle = |N-1,1,0,0\rangle_{gesa}$, $|1\rangle_L = |\mathbf{s}\rangle = |N-1,0,1,0\rangle_{gesa}$, $|\mathbf{a}_+\rangle = |N-1,0,0,1\rangle_{gesa}\}$. The coupling diagram of the ensemble of atoms is equivalent to a simple three-state coupling diagram for a single atom, as shown in Fig. 3.

Representing the Hamiltonian in matrix form in this basis, we have

$$H_1(t) = \begin{bmatrix} 0 & \Omega\sin\theta & -\Omega\cos\theta e^{i\varphi} \\ \Omega\sin\theta & 0 & 0 \\ -\Omega\cos\theta e^{-i\varphi} & 0 & 0 \end{bmatrix}. \tag{3}$$

The zero-energy eigenspace of the Hamiltonian is non-degenerate. The dark state is

$$|D(t)\rangle = \cos\theta|1\rangle_L + \sin\theta e^{-i\varphi}|\mathbf{a}_+\rangle. \tag{4}$$

Note that the Hamiltonian is decoupled from the state $|0\rangle_L = |N,0,0,0\rangle_{grsa}$.

Assume the initial state is $|\psi(-\infty)\rangle = |D(-\infty)\rangle = |1\rangle_L$ (which means $\theta(-\infty) = 0$ at the very beginning). Also, assume that initially $\varphi = 0$. Now, turn on two laser beams, using the standard formula to calculate the geometric phase, where the parameters make a cyclic evolution with the starting and ending point $\theta = 0, \varphi = 0$:

$$\phi_1 = i\oint \mathrm{d}\mathbf{R}\langle D(t)|\nabla_{\mathbf{R}}|D(t)\rangle, \tag{5}$$

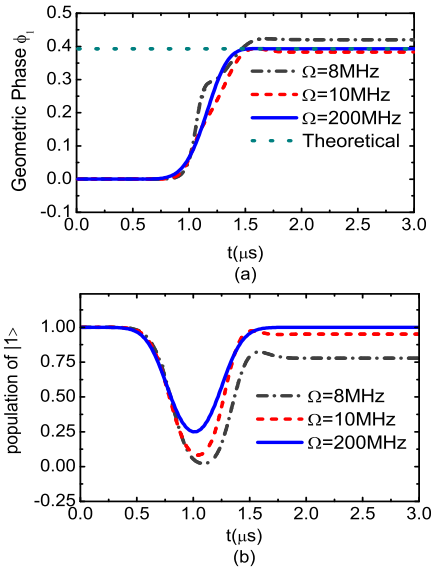

FIG. 4: (Color online.) (a) The evolution of the relative phase between state $|1\rangle_L$ and state $|0\rangle_L$ for three different values of Ω, to realize a $\pi/16$ gate. Note that after the cyclic evolution, we get an additional pure geometric phase, which fits the theoretical value quite well for Ω larger than 200MHz. (b) The population change of state $|1\rangle_L$ during the process. We can see that only if Ω is large enough to satisfy the adiabatic condition can we get high accuracy of the gate. Two short laser pulses are determined by $\theta(t) = \frac{\pi}{3}\exp((t-1)^2/0.15)$ and $\varphi(t) = \frac{\pi}{3}\exp((t-1.5917)^2/0.15)$ (the unit of t is μs).

where $\mathbf{R}(t) = (\theta(t), \varphi(t))$. We have

$$\langle D(t)|\nabla_{\mathbf{R}}|D(t)\rangle = -i\sin^2(\theta)\hat{\varphi}$$

and

$$\phi_1 = \oint \sin^2(\theta)\mathrm{d}\varphi.$$

According to Green's theorem, this geometric phase is exactly the enclosed solid angle:

$$\phi_1 = \iint_{\partial S}\sin\theta\mathrm{d}\theta\mathrm{d}\varphi = \iint_{\partial S}\mathrm{d}\Omega.$$

A pulse sequence consisting of two stimulated Raman adiabatic passage (STIRAP) pulses with relatively large width (to guarantee that the process is adiabatic) can be used for this purpose.

A numerical simulation of resonance coupling to realize a $\pi/16$ gate ($\phi_1 = \pi/8$) is shown in Fig. 4. Since in the laboratory the Rabi frequency Ω can be as high as 200 MHz, the adiabatic process could be finished in several microseconds, which is much shorter than the decoherence time of the hyperfine ground states. We can exchange the population of $|1\rangle_L$ and $|\mathbf{a}_+\rangle$ back and forth without losing any information, and we can get a geometric phase with high accuracy if Ω is large enough.

In the previous method of using ensembles of atoms or molecules to realize quantum information processing, a major shortcoming is that it is very hard to uniformly illuminate all the atoms, thus limiting the accuracy of the gate operation. But in our proposal, each atoms interacts individually with Ω_1 and Ω_a, and the geometric phase is independent of the absolute value of Ω. If the spatial distribution of the electric fields of the two laser beams match each other, say $\widetilde{\Omega}_1(\mathbf{r}) = \widetilde{E}_1(\mathbf{r})d_{es} = \widetilde{E}_a(\mathbf{r})d_{ea_+} = \widetilde{\Omega}_a(\mathbf{r})$ for every point in space $\mathbf{r}$, the effect of non-uniform illumination can be naturally eliminated. This is an advantage of adiabatic control.

B. Y-Rotation Gate

Now we show how to achieve the gate $U = e^{i\phi_2\sigma_y}$. This gate is much more complicated to realize than the one-qubit phase gate. It is difficult to couple the state $|0\rangle_L$ to $|1\rangle_L$, since directly coupling them by applying a laser beam to the ensemble of atoms would result in unwanted higher collective excitations. In Ref. [14], a scheme taking advantage of the dipole-dipole interaction of Rydberg states between atoms was used to realize this gate. Here we propose a geometric gate by following three steps:

1. Adiabatically pump the ground state $|0\rangle_L$ to a highly excited Rydberg state $|\mathbf{r}\rangle$, using the dipole-dipole interaction to assure that only a single collective excitation is achieved.

2. Adiabatically control the coupling between the single excitation states $|\mathbf{r}\rangle$, $|\mathbf{s}\rangle$, and $|\mathbf{a}_+\rangle$ to geometrically realize the gate.

3. Reverse step 1 to transfer $|\mathbf{r}\rangle$ back to $|0\rangle_L$.

To carry out step 1, consider Rydberg states of a hydrogen atom within a manifold of fixed principle quantum number n with degeneracy n^2. This degeneracy can be removed by applying a constant electric field E along a certain axis (linear Stark effect), such as the z axis. For electric fields below the Ingris-Teller limit, the mixing of adjacent n manifolds can be ignored, and energy levels are split according to $\Delta E_{nqm} = 3nqea_BE/2$ with parabolic and magnetic quantum numbers q and m, respectively. Here, q can take values $n-1-|m|, n-3-|m|, ..., -(n-1-|m|)$, e is the electron charge, and a_B the Bohr radius. These states have dipole moments of $\mu = 3nqea_B\mathbf{e}_z/2$.

Consider two atoms k and l seperated by a distance $\mathbf{R}$. The dipole-dipole interaction between them is

$$V_{\rm dip}^{kl}(\mathbf{R}) = \frac{1}{4\pi\epsilon_0}\left[\frac{\hat{\mu}_k\cdot\hat{\mu}_l}{|\mathbf{R}|^3} - 3\frac{(\hat{\mu}_k\cdot\mathbf{R})(\hat{\mu}_l\cdot\mathbf{R})}{|\mathbf{R}|^5}\right], \qquad (6)$$

where $\hat{\mu}_k$ and $\hat{\mu}_l$ are dipole moment operators for atoms k and l. Suppose the electric field is sufficiently large that the energy splitting between two adjacent Stark states is much larger than the dipole-dipole interaction.

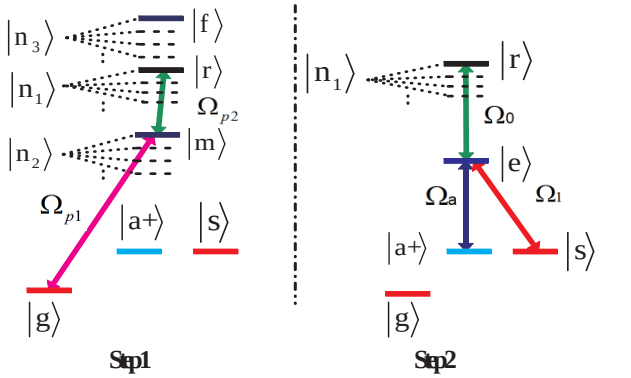

FIG. 5: (Color online.) The level diagram with the couplings to realize the $R_y^i(\phi)$ gate. We apply an electric field to the ensemble of atoms, and pick appropriate Stark eigenstates of rubidium to be the register states $|r\rangle = |r\rangle_{70,0}$, $|f\rangle = |r\rangle_{72,0}$ and the intermediate Rydberg state $|m\rangle = |r\rangle_{60,0}$ as shown the Appendix. States $|g\rangle$, $|a_+\rangle$ and $|s\rangle$ are the in the same manifold of the internal ground state. In the first step, two conjugate laser beams Ω_{p1} and Ω_{p2} are used to adiabatically pump a single excitation from $|\mathbf{g}\rangle$ to $|\mathbf{r}\rangle$. In the second step, three laser beams Ω_0, Ω_1, Ω_a are used to adiabatically realize the $R_y^i(\phi)$ gate. The excitation from $|g\rangle$ to $|r\rangle$ is then adiabatically reversed.

For two atoms initialized in Stark eigenstates, the diagonal terms of $V_{\rm dip}^{kl}(\mathbf{R})$ provide an energy shift, while the nondiagonal terms couple adjacent m manifolds with each other, $(m,m) \to (m\pm1, m\mp1)$. The off-diagonal transition can cause decoherence, and is suppressed by an appropriate choice of initial Stark eigenstate [7]. (For hydrogen, the state is $|r\rangle_n = |n, q = n-1, m = 0\rangle$.) For a fixed distance $\mathbf{R} = \mathrm{R}\mathbf{e}_z$, the dipole-dipole interaction of two atoms k and l in the states $|r_k\rangle_{n_1}$ and $|r_l\rangle_{n_2}$ is

$$\begin{aligned} u_{n_1n_2}^{kl}(\mathrm{R}) &= {}_{n_1}\langle r_k|_{n_2}\langle r_l|V_{\rm dip}^{kl}(\mathbf{R})|r_k\rangle_{n_1}|r_l\rangle_{n_2} \\ &= -\frac{9a_B^2e^2}{R^3 8\pi\epsilon_0}[n_1n_2(n_1-1)(n_2-1)]. \end{aligned}$$

For n_1 and n_2 sufficiently large, $u(\mathrm{R}) \propto n_1^2n_2^2$. For alkali atoms such as rubidium, the situation is more complicated, but this kind of analysis still works. In the Appendix, we discuss how to pick a state which has characteristics similar to $|r\rangle_n$ for rubidium. We will make use of this energy shift later.

Consider the diagram shown in Fig. 5. For step 1, there should be a single excitation in state $|r\rangle$ after pumping if the initial state is $|0\rangle_L$, and no excitation in state $|r\rangle$ if the initial state is $|1\rangle_L$. To achieve this goal, we introduce two other Rydberg states $|m\rangle$ and $|f\rangle$, and adiabatically transfer the amplitude of $|1\rangle_L$ to $|\mathbf{f}\rangle$ by coupling $|s\rangle$ and $|f\rangle$ to some intermediate state. Note that this pumping process can also be realized adiabatically. This process would also be used when we do measurement; more details will be given in the measurement section.

The Hamiltonian of the cloud of atoms as described in the left side of Fig. 5 in the rotating wave approximation is:

$$\begin{aligned} H_p(t) = &\sum_i (\Omega_{p1}(t)\sigma_{gm}^{(i)} + \text{H.c}) \\ &+ \sum_i (\Omega_{p2}(t)\sigma_{mr}^{(i)} + \text{H.c}) \\ &+ \sum_{k>l} \Big(u_{mm}^{kl}(\mathbf{R}_{kl})|m_k\rangle|m_l\rangle\langle m_k|\langle m_l| \\ &\quad + u_{rr}^{kl}(\mathbf{R}_{kl})|r_k\rangle|r_l\rangle\langle r_k|\langle r_l| \Big) \\ &\quad + u_{ff}^{kl}(\mathbf{R}_{kl})|f_k\rangle|f_l\rangle\langle f_k|\langle f_l| \\ &\quad + u_{rm}^{kl}(\mathbf{R}_{kl})|r_k\rangle|m_l\rangle\langle r_k|\langle m_l| \\ &\quad + u_{fm}^{kl}(\mathbf{R}_{kl})|f_k\rangle|m_l\rangle\langle f_k|\langle m_l| \\ &\quad + u_{fr}^{kl}(\mathbf{R}_{kl})|f_k\rangle|r_l\rangle\langle f_k|\langle r_l| \Big). \end{aligned} \tag{7}$$

The two-body interaction term here is due to the energy shift of the states. Just as in the case of the phase gate, we represent the Hamiltonian in second quantized form. Again, assuming the laser fields are uniformly coupled to each atom, and using the standard second quantization procedure to deal with the two-body interaction, we apply the minimum energy shift for all pairs of atoms (as the worst case) and obtain

$$\begin{aligned} H_p^{\text{eff}}(t) \approx &\Omega_{p1}(t)\sqrt{N}(\hat{\mathcal{M}}^\dagger + \hat{\mathcal{M}}) \\ &+ \Omega_{p2}(t)(\hat{\mathcal{R}}\hat{\mathcal{M}}^\dagger + \hat{\mathcal{R}}^\dagger\hat{\mathcal{M}}) \\ &+ \overline{u}_{mm}\hat{\mathcal{M}}^\dagger\hat{\mathcal{M}}^\dagger\hat{\mathcal{M}}\hat{\mathcal{M}} + \overline{u}_{rr}\hat{\mathcal{R}}^\dagger\hat{\mathcal{R}}^\dagger\hat{\mathcal{R}}\hat{\mathcal{R}} \\ &+ \overline{u}_{ff}\hat{\mathcal{F}}^\dagger\hat{\mathcal{F}}^\dagger\hat{\mathcal{F}}\hat{\mathcal{F}} + \overline{u}_{rm}\hat{\mathcal{R}}^\dagger\hat{\mathcal{R}}\hat{\mathcal{M}}^\dagger\hat{\mathcal{M}} \\ &+ \overline{u}_{fm}\hat{\mathcal{F}}^\dagger\hat{\mathcal{F}}\hat{\mathcal{M}}^\dagger\hat{\mathcal{M}} + \overline{u}_{fr}\hat{\mathcal{F}}^\dagger\hat{\mathcal{F}}\hat{\mathcal{R}}^\dagger\hat{\mathcal{R}}, \end{aligned} \tag{8}$$

where $\overline{u}_{rr}$, $\overline{u}_{mm}$, $\overline{u}_{ff}$, $\overline{u}_{rm}$, $\overline{u}_{fm}$ and $\overline{u}_{fr}$ are chosen to be the minimum energy shifts from the dipole-dipole interaction.

In the case of low excitation, in the Bogoliubov approximation we can regard the operators $\mathcal{G}, \mathcal{G}^\dagger$ on state $|g\rangle$ as the C-number $\sqrt{N}$, where N is the total number of the atoms in the cloud. When the system is initially in $|0\rangle_L$ (and hence $|f\rangle$ is not excited), the equivalent state coupling diagram for this pumping process is shown in Fig. 6(a). Unlike the phase gate, we see that this Hamiltonian is no longer closed in a small subspace of states because Ω_{p1} will continuously pump atoms of the ensemble from the ground state to the excited states. However, because of the large energy shift, the rate to excite $|N-2,1,0,1\rangle_{grsm}$ and $|N-2,1,1,0\rangle_{grsm}$ is strongly suppressed. Physically, this means there cannot be an atom excited to the Rydberg state $|r\rangle$ while another atom be excited to state $|i\rangle$ or $|m\rangle$. Only a single excitation to the register state can be achieved ($|0\rangle_L \rightarrow |\mathbf{r}\rangle$) during this adiabatic process.

If the system is initially in the state $|1\rangle_L$ (and hence there is a single excitation in $|f\rangle$), both $|r\rangle$ and $|m\rangle$ cannot be excited due to the energy shift caused by the dipole-dipole interaction, as shown in Fig. 6(b). A numerical simulation of the pumping process for the minimum energy shift is shown in Fig. 7.

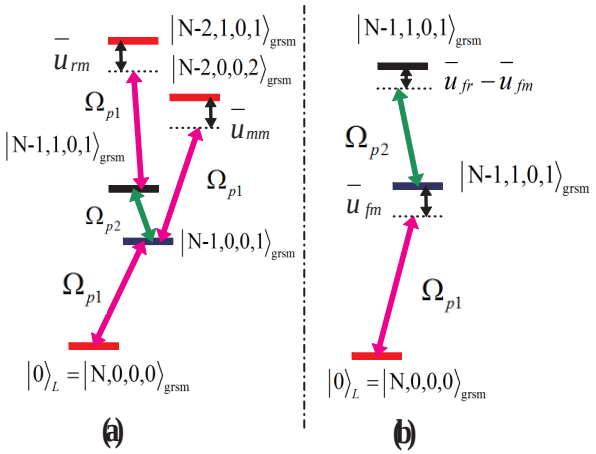

FIG. 6: (Color online.) The equivalent coupling diagram of the ensembles of atoms in cases of collective excitation for the case (a) system is initially in $|0\rangle_L$ and (b) system is initially in $|1\rangle_L$.

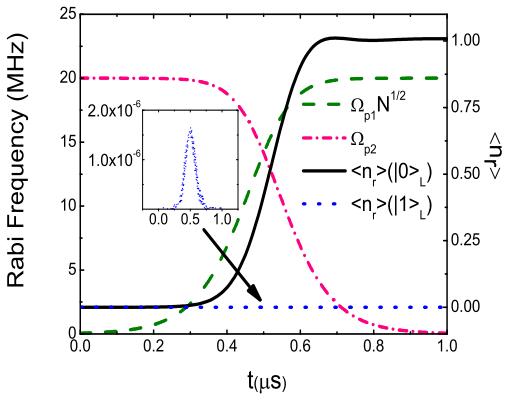

FIG. 7: (Color online.) Adiabatic Pumping process. Note that at the end there is only a single excitation in the register state $|r\rangle$ when initially in $|0\rangle_L$, and no excitation when initially in $|1\rangle_L$. Here, we set $\overline{\mu}_{rm} = 400$MHz and $\overline{\mu}_{mm} = 300$MHz. Since we take the minimum energy shift as our simulation parameter, the actual performance should be better (i.e., the process could be finished in a shorter period of time).

After the pumping process, and the adiabatic transfer of the population of $|\mathbf{f}\rangle$ back to $|1\rangle_L$, we can then realize the $R_y^i(\phi)$ gate on the ensemble of atoms by applying three controlling laser beams. The coupling diagram is shown in the right side of Fig. 5. The Hamiltonian of step 2 can be obtained directly in second-quantized form:

$$\begin{aligned} H_2(t) = &\Omega_0(t)(\hat{\mathcal{E}}\hat{\mathcal{R}}^\dagger + \hat{\mathcal{E}}^\dagger\hat{\mathcal{R}}) + \Omega_1(t)(\hat{\mathcal{E}}\hat{\mathcal{S}}^\dagger + \hat{\mathcal{E}}^\dagger\hat{\mathcal{S}}) \\ &+ \Omega_a(t)(\hat{\mathcal{E}}\hat{\mathcal{A}}_+^\dagger + \hat{\mathcal{E}}^\dagger\hat{\mathcal{A}}_+). \end{aligned} \tag{9}$$

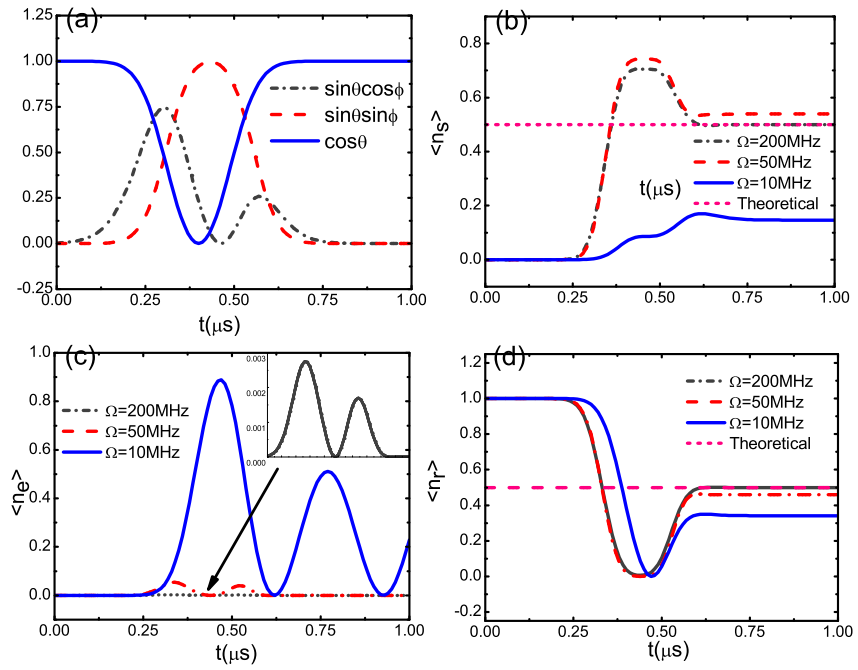

FIG. 8: (Color online.) (a): The pulse shape of the control lasers of Ω_0, Ω_1 and Ω_a respectively. (b), (c), (d): The evolution of the populations of $|s\rangle$, $|e\rangle$, $|r\rangle$. We see that when Ω is larger than 200MHz, the adiabatic condition is satisfied, the gate works with very high accuracy (close to the theoretical value), and the population of the short-lived state $|e\rangle$ tends to zero.

We can directly apply the technique of geometric transformations to realize this gate, as introduced in Ref. [21] for four-level systems. Here, we choose $\Omega_0 = \Omega\sin\theta\cos\varphi$, $\Omega_1 = \Omega\sin\theta\sin\varphi$, $\Omega_a = \Omega\cos\theta$. This time, the Hamiltonian is closed in the basis $\{|\mathbf{e}\rangle, |0\rangle_L = |\mathbf{r}\rangle, |1\rangle_L = |\mathbf{s}\rangle, |\mathbf{a}_+\rangle\}$:

$$H_2(t) = \Omega \begin{bmatrix} 0 & \sin\theta\cos\varphi & \sin\theta\sin\varphi & \cos\theta \\ \sin\theta\cos\varphi & 0 & 0 & 0 \\ \sin\theta\sin\varphi & 0 & 0 & 0 \\ \cos\theta & 0 & 0 & 0 \end{bmatrix}. \tag{10}$$

The eigenspace corresponding to the zero-energy eigenvalue (dark space) is spanned by basis vectors $\{|D_1\rangle$, and $|D_2\rangle\}$, where

$$|D_1\rangle = \sin\varphi|0\rangle_L - \cos\varphi|1\rangle_L,$$

$$|D_2\rangle = \cos\theta(\cos\varphi|0\rangle_L + \sin\varphi|1\rangle_L) - \sin\theta|\mathbf{a}_+\rangle.$$

We can use the formula for the degenerate subspace under the cyclic evolution of θ, φ. Suppose $|\psi(t)\rangle = C_1(t)|D_1\rangle + C_2(t)|D_2\rangle$. We have the equation

$$\begin{bmatrix} \dot{C}_1 \\ \dot{C}_2 \end{bmatrix} = \begin{bmatrix} D_{11}(t) & D_{12}(t) \\ D_{21}(t) & D_{22}(t) \end{bmatrix} \begin{bmatrix} C_1 \\ C_2 \end{bmatrix}, \tag{11}$$

where $D_{ij}(t) = \langle D_i|\dot{D}_j\rangle$. Let's define

$$\begin{aligned} dA_2(t) &= \begin{bmatrix} D_{11}(t) & D_{12}(t) \\ D_{21}(t) & D_{22}(t) \end{bmatrix} dt \\ &= \begin{bmatrix} 0 & -\cos\theta\dot{\varphi} \\ \cos\theta\dot{\varphi} & 0 \end{bmatrix} dt, \end{aligned} \tag{12}$$

and also the unitary matrix

$$\mathcal{U} = \mathcal{P}\exp(i\oint_{\mathbf{C}} dA_2(t)). \tag{13}$$

After the cyclic evolution,

$$\begin{aligned} |D_1(T)\rangle &= \mathcal{U}^{11}|D_1(0)\rangle + \mathcal{U}^{21}|D_2(0)\rangle, \\ |D_2(T)\rangle &= \mathcal{U}^{12}|D_1(0)\rangle + \mathcal{U}^{22}|D_2(0)\rangle. \end{aligned} \tag{14}$$

At the beginning, if we set $\theta(0) = 0$ and $\varphi(0) = \frac{\pi}{2}$, we will have $|D_1(0)\rangle = |0\rangle_L$ and $|D_2(0) = |1\rangle_L$. We can use the Dyson expansion to get the unitary matrix $\mathcal{U}$. This gives us:

$$\begin{aligned} \mathcal{U}^{11} &= 1 - \frac{\phi_2^2}{2} + \frac{\phi_2^4}{24} - \frac{\phi_2^6}{720}... = \cos\phi_2, \\ \mathcal{U}^{12} &= \phi_2 - \frac{\phi_2^3}{6} + \frac{\phi_2^5}{120}... = \sin\phi_2, \\ \mathcal{U}^{21} &= -\phi_2 + \frac{\phi_2^3}{6} - \frac{\phi_2^5}{120}... = -\sin\phi_2, \\ \mathcal{U}^{22} &= 1 - \frac{\phi_2^2}{2} + \frac{\phi_2^4}{24} - \frac{\phi_2^6}{720}... = \cos\phi_2, \end{aligned} \tag{15}$$

where

$$\phi_2 = \oint_{\mathbf{C}} \cos\theta \mathrm{d}\varphi$$

is a pure geometric phase. Thus we get the unitary transformation we want. Step 3 is simply the reverse of step 1, to return us to our original basis.

A simulation to realize $\phi_2 = \pi/4$ was done for a certain pulse shape of the coupling laser beams, where the qubit was initially prepared in the state $|0\rangle_L$, as shown in Fig. 8(a). We show the evolution of the populations of states $|s\rangle$, $|e\rangle$ and $|r\rangle$ in Fig. 8(b), (c), and (d), respectively. If Ω is large enough ($\geq$ 200 MHz, which is practical in current experiments), we could implement the gate operation in 1μs with extremely high accuracy. Thus, the total procedure takes less than 5μs to complete, while the lifetime of $|\mathbf{r}\rangle$ is approximately equal to the lifetime of $|r\rangle$ [11], which is estimated to be 300-400μs in a cryogenic environment [35].

We simplified the calculation and simulation by assuming that all atoms are uniformly illuminated in the laser beam. However, just like the argument made in the previous section, the geometric phase is independent for large Ω, if the spatial distribution of the electric fields of the three laser beams match each other at each point in space. Thus, we can in principal eliminate the error introduced by nonuniform illumination.

C. Two-Qubit Controlled Phase Gate

Now, we are ready to construct the controlled phase gate. Recently, an adiabatic SWAP operation between states of two clouds of atoms in a cavity QED system was experimentally achieved [36]. Here, we extend this method to geometrically realize the controlled phase gate, which together with the earlier one-qubit gates gives a universal set of quantum gates. The basic idea is to couple two qubits (that is, clouds of atoms) by virtually emitting and absorbing a cavity photon; and after an adiabatic evolution, the second qubit obtains an extra relative phase when the first qubit is in $|0\rangle_L$. The coupling diagram of the scheme is shown in Fig. 9.

Suppose the length of the cavity is about 200μm, which means, it could contain about 10 qubits. Consider two different clouds of atoms in the cavity. For a single atom in each cloud, pick a manifold of states of p. When an electric field is applied to these two cloud of atoms, the manifold splits into $|r_+\rangle$ and $|r_-\rangle$. For atom cloud 1, we set a constant electrical field E_{z1} and a constant magnetic field B_{z1} in the z direction. The Stark Effect splits the manifold p, and the Zeeman effect changes the energy of $|g\rangle$ and $|s\rangle$.

Assume the energy difference between $|g\rangle$ and $|s\rangle$ to be δ. Set the appropriate non-zero value of E_{z1} and B_{z1} so that $|r_+\rangle$ is resonantly coupled to $|g\rangle$ and $|s\rangle$ by a cavity mode a and a control laser Ω_1 respectively. For atom cloud 2, E_{z2} is set so that $|r_+\rangle$ is resonantly coupled to

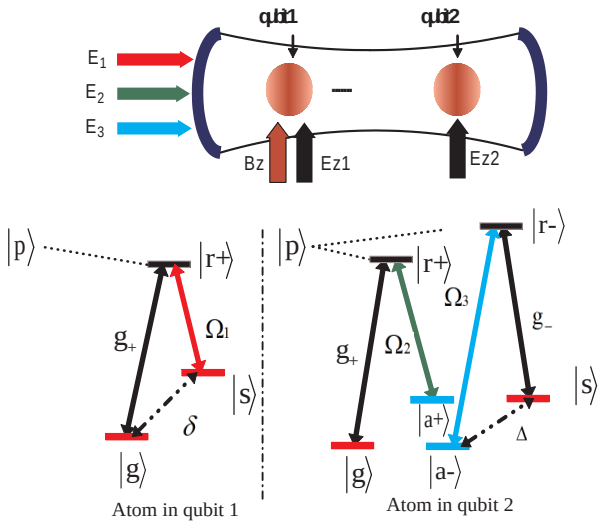

FIG. 9: (Color online.) The schematic setup to realize the conditional phase gate, and the relevant atomic levels of the two clouds of atoms.

$|g\rangle$ and $|s\rangle$ by the same cavity mode a and control laser Ω_2, and $|r_-\rangle$ is resonantly coupled to $|s\rangle$ and $|a_-\rangle$ by the cavity mode and a control laser Ω_3. Note that for Rb^{87}, the hyperfine structure energy split of the ground state manifold is $\Delta/2\pi$=6.835GHz, and the energy difference of $|r_+\rangle$ and $|r_-\rangle$ should set to be equal to Δ for atom cloud 2 for the purpose of resonant coupling, while the frequencies of Ω_1, Ω_2 and Ω_3 should be $\omega_{\rm cav}-\delta$, $\omega_{\rm cav}-\Delta$ and $\omega_{\rm cav}+\Delta$, respectively, where $\omega_{\rm cav}$ is the frequency of cavity mode.

Since the cavity mode is inhomogeneously distributed, the thermal motion (even at extremely low temperature) of atoms, causes the coupling rate between atoms and cavity photons to vary greatly from one to another (by roughly a factor of 2) and thus makes the system difficult to control accurately. To overcome these difficulties, instead of directly applying the laser beam to the clouds of atoms, we use the idea of external laser driving control [37] as shown in schematic setup in Fig. 9. Three classical laser fields $E_1(t)$, $E_2(t)$ and $E_3(t)$ are incident on one mirror of the cavity to drive the transition $|r_+\rangle \rightarrow |s\rangle$ for cloud 1, and $|r_+\rangle \rightarrow |a_+\rangle$ and $|r_-\rangle \rightarrow |a_-\rangle$ for cloud 2, through another cavity mode a'. We assume for simplicity that a and a' have the same spatial mode structure $\chi(\mathbf{r})$ with the same frequency $\omega_{\rm cav}$, so they can be different only in polarization.

The driving fields $E_1(t)$, $E_2(t)$ and $E_3(t)$ are resonant with frequencies $\omega_{\rm cav}-\delta$, $\omega_{\rm cav}-\Delta$ and $\omega_{\rm cav}+\Delta$. So they are far off-resonant to the cavity mode. $E_1(t)$, $E_2(t)$ and $E_3(t)$ control the time evolution of the Rabi frequencies Ω_1, Ω_2 and Ω_3. To see this, consider the input-output equation for the cavity mode a' [38]:

$$\frac{da'(t)}{dt} = -i[a(t), H_{sys}] - \frac{\kappa}{2}a'(t) + \sqrt{\kappa}a'_{\rm in}(t), \qquad (16)$$

where $a'_{\rm in}(t)$ is the field operator for the input driving pulse coupling to the mode a', with

$$\langle a'_{\rm in}(t)\rangle = E_1(t) + E_2(t) + E_3(t),$$

and

$$[a'_{\rm in}(t), a'^{\dagger}_{\rm in}(t')] = \delta(t-t').$$

Since a' is driven by strong classical pulses, we can treat the mode as classical and thus assume that the interaction between a' and the atoms will not change the state of the cavity mode a'. Eq. (16) therefore can be modified to be

$$\begin{aligned}\frac{da'(t)}{dt} =& -i\omega_{\rm cav}a'(t) - \frac{\kappa}{2}a'(t) \\ &+ \sqrt{\kappa}(E_1(t) + E_2(t) + E_3(t)).\end{aligned} \tag{17}$$

First, we suppose there is only one classical pulse $E_1(t) = \langle a'_{\rm in}(t)\rangle = \varepsilon_1(t)e^{-i(\omega_{\rm cav}-\delta)t}$, where $\varepsilon_1(t)$ is the slowly varying amplitude of $E_1(t)$. Then, we can write the mean value of a' as

$$\langle a'(t)\rangle = \alpha(t)e^{-i(\omega_{\rm cav}-\delta)t},$$

which has the solution

$$\begin{aligned}\alpha(t) &= \int_0^t \varepsilon_1(\tau)\exp(-i\delta-\kappa/2)(t-\tau)d\tau \\ &\approx \frac{\varepsilon_1(t) - e^{(-i\delta-\kappa/2)t}\varepsilon_1(0)}{i\delta+\kappa/2}\end{aligned} \tag{18}$$

when the characteristic time T_1 of $\varepsilon_1(t)$ satisfies $\delta T_1 \gg 1$.

Assume that $\varepsilon_1(t)$ gradually increases from zero with $\varepsilon_1(0) = 0$. Then $\alpha(t) \propto \varepsilon_1(t)$. By choosing an appropriate phase of $\varepsilon_1(t)$, we set $\alpha(t)$ to be real. If we input $E_2(t)$ or $E_3(t)$, the solution will have a similar form. Now, consider the case when three classical pulses are incident on the cavity mirror. Eq. (16) is a linear equation, so, when the three input pulse have different resonant frequencies, the solution should be a superposition of the solutions for three single pulses. Thus, we can represent $\langle a'(t)\rangle$ as

$$\begin{aligned}\langle a'(t)\rangle \;=\; & \alpha_1(t)e^{-i(\omega_{\rm cav}-\delta)t} + \alpha_2(t)e^{-i(\omega_{\rm cav}-\Delta)t} \\ & +\alpha_3(t)e^{-i(\omega_{\rm cav}+\Delta)t}.\end{aligned}$$

This gives Rabi frequencies $\Omega_i(\mathbf{r},t) = d_i\alpha_i(t)\chi(\mathbf{r})$ for $i = 1,2,3$, where d_i is a coefficient mainly determined by the dipole moment for the corresponding transition.

The frequencies of the three components of a' differ significantly, so we can regard them as three separate pulses. In addition, the energy structure of atoms in cloud 1 is different from those in cloud 2, so Ω_1 will not interact with the atoms in cloud 2. Similarly, Ω_2 and Ω_3 will not interact with atoms in cloud 1. All other clouds in the cavity are far off-resonant from both the cavity mode and the control lasers, and thus can be safely excluded by our gate operation. Now, we can represent the Hamiltonian for the situation of Fig. 9 in the interaction picture:

$$\begin{aligned}H_3(t) =& \sum_{j_1}\Omega_1(\mathbf{r}_{j_1},t)\sigma^{(j_1)}_{sr_+} + \sum_{j_1} g_+(\mathbf{r}_{j_1})a^\dagger\sigma^{(j_1)}_{gr_+} \\ &+ \sum_{j_2}(\Omega_2(\mathbf{r}_{j_2},t)\sigma^{(j_2)}_{a_+r_+} + \Omega_3(\mathbf{r}_{j_2},t)\sigma^{(j_2)}_{a_-r_-}) \\ &+ \sum_{j_2}(g_+(\mathbf{r}_{j_2})a^\dagger\sigma^{(j_2)}_{gr_+} + g_-(\mathbf{r}_{j_2})a^\dagger\sigma^{(j_2)}_{sr_-}) \\ &+ \text{H.c.}\end{aligned} \tag{19}$$

where a and $a^\dagger$ are annihilation and creation operators of cavity mode a, and $g_+(\mathbf{r})$ and $g_-(\mathbf{r})$ are coupling rates of cavity mode a to the transition $|g\rangle \to |r_+\rangle$ in cloud 1 and $|s\rangle \to |r_-\rangle$ in cloud 2. We can represent $g_+(\mathbf{r})(g_-(\mathbf{r})) = \widetilde{g}_+\chi(\mathbf{r})(\widetilde{g}_-\chi(\mathbf{r}))$, where $\widetilde{g}_+$ and $\widetilde{g}_-$ are constants. So we can rewrite the Hamiltonian as:

$$\begin{aligned}H_3(t) =& \sum_{j_1}\chi(\mathbf{r}_{j_1})(d_1\alpha_1(t)\sigma^{(j_1)}_{sr_+} + \widetilde{g}_+a^\dagger\sigma^{(j_1)}_{gr_+}) \\ &+ \sum_{j_2}\chi(\mathbf{r}_{j_2})(d_2\alpha_2(t)\sigma^{(j_2)}_{a_+r_+} + d_3\alpha_3(t)\sigma^{(j_2)}_{a_-r_-} \\ &+ \widetilde{g}_+a^\dagger\sigma^{(j_2)}_{gr_+} + \widetilde{g}_-a^\dagger\sigma^{(j_2)}_{sr_-}) + \text{H.c.},\end{aligned} \tag{20}$$

We will see soon that the dark state of such a Hamiltonian should be independent of $\chi(\mathbf{r})$, and the adiabatic evolution of the system is determined only by the minimum value of $\chi(\mathbf{r}_j)$ for all j, say χ_m. So, the Hamiltonian can effectively be represented as:

$$\begin{aligned}H_3^{\rm eff}(t) =& \sum_{j_1}(\Omega_1(t)\sigma^{(j_1)}_{sr_+} + g_+a^\dagger\sigma^{(j_1)}_{gr_+}) \\ &+ \sum_{j_2}(\Omega_2(t)\sigma^{(j_2)}_{a_+r_+} + \Omega_3(t)\sigma^{(j_2)}_{a_-r_-}) \\ &+ \sum_{j_2}(g_+a^\dagger\sigma^{(j_2)}_{gr_+} + g_-a^\dagger\sigma^{(j_2)}_{sr_-}) + \text{H.c.},\end{aligned} \tag{21}$$

where $\Omega_i(t) = d_i\alpha_i(t)\chi_m$ for $i = 1,2,3$ and $g_+(g_-) = \widetilde{g}_+\chi_m(\widetilde{g}_-\chi_m)$. As in the previous cases, we transform the Hamiltonian to second quantized representation. For two clouds of atoms in the Bogoliubov approximation, we get the new Hamiltonian

$$\begin{aligned}H_3^{\rm eff}(t) \approx& \Omega_1(t)(\hat{\mathcal{S}}^\dagger)_1(\hat{\mathcal{R}}_+)_1 + \Omega_2(t)(\hat{\mathcal{A}}^\dagger_+)_2(\hat{\mathcal{R}}_+)_2 \\ &+ \Omega_3(t)(\hat{\mathcal{A}}^\dagger_-)_2(\hat{\mathcal{R}}_-)_2 + g_+\sqrt{N}a^\dagger(\hat{\mathcal{R}}_+)_1 \\ &+ g_+\sqrt{N}a^\dagger(\hat{\mathcal{R}}_+)_2 + g_-a^\dagger(\hat{\mathcal{S}}^\dagger)_2(\hat{\mathcal{R}}_-)_2 + \text{H.c.},\end{aligned} \tag{22}$$

where $\hat{\mathcal{S}}$, $\hat{\mathcal{R}}_-$, $\hat{\mathcal{R}}_+$, $\hat{\mathcal{A}}_-$, and $\hat{\mathcal{A}}_+$ are the bosonic annihilation operators of the single atom states $|s\rangle$, $|r_-\rangle$, $|r_+\rangle$, $|a_-\rangle$, and $|a_+\rangle$, respectively. We set

$$\begin{aligned}\Omega_1(t) =& \Omega_1\sin\theta e^{-i\varphi_1}, \\ \Omega_2(t) =& \Omega_2\cos\theta e^{-i\varphi_2}, \\ \Omega_3(t) =& \Omega_3\cos\theta e^{-i\varphi_3}.\end{aligned}$$

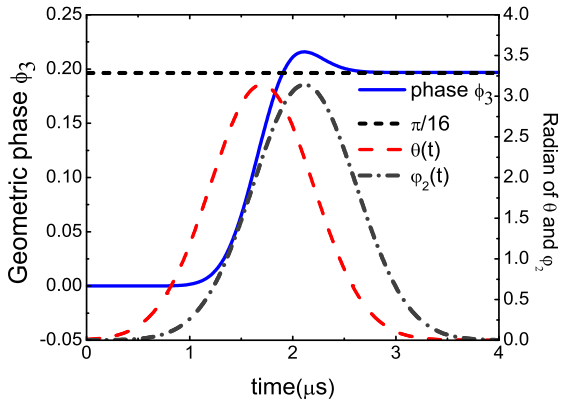

FIG. 10: (Color online.) The evolution of the phase ϕ_3 of $|10\rangle_L$. The pulse shapes of $\theta(t)$ and $\varphi(t)$ are also given.

We also define $g_1 = g_+\sqrt{N}$, $g_2 = g_+\sqrt{N}$ and $g_3 = g_-$ for convenience.

As in the previous sections, for each cloud of atoms we have a set of basis states:

$$\begin{aligned}
|0\rangle_L &= |N,0,0,0,0,0\rangle_{gr_+r_-a_+a_-s},\\
|1\rangle_L &= |N-1,0,0,0,0,1\rangle_{gr_+r_-a_+a_-s},\\
|\mathbf{r}_+\rangle &= |N-1,1,0,0,0,0\rangle_{gr_+r_-a_+a_-s},\\
|\mathbf{r}_-\rangle &= |N-1,0,1,0,0,0\rangle_{gr_+r_-a_+a_-s},\\
|\mathbf{a}_+\rangle &= |N-1,0,0,1,0,0\rangle_{gr_+r_-a_+a_-s},\\
|\mathbf{a}_-\rangle &= |N-1,0,0,0,1,0\rangle_{gr_+r_-a_+a_-s}.
\end{aligned}$$

The Hamiltonian is closed in a subspace of Hilbert space that can be divided into the direct sum of two closed subspaces:

$$\mathcal{H} = (\mathcal{H}^1 \otimes \mathcal{H}^2_+) \oplus (\mathcal{H}^1 \otimes \mathcal{H}^2_-). \tag{23}$$

Here, $\mathcal{H}^1 \otimes \mathcal{H}^2_+$ is spanned by basis vectors $\{|100\rangle, |\mathbf{r}_+00\rangle, |001\rangle, |0\mathbf{r}_+0\rangle, |0\mathbf{a}_+0\rangle\}$, and $\mathcal{H}^1 \otimes \mathcal{H}^2_-$ is spanned by basis vectors $\{|110\rangle, |\mathbf{r}_+10\rangle, |011\rangle, |0\mathbf{r}_-0\rangle, |0\mathbf{a}_-0\rangle\}$. The first two degrees of freedom represent cloud 1 and cloud 2, and the last degree of freedom of the state is the Fock state of the cavity photons. Since the Hamiltonian doesn't couple these two subspaces, and has the same form in each subspace, we can just consider a single subspace, e.g., $\mathcal{H}^1 \otimes \mathcal{H}^2_+$. The Hamiltonian can be represented in this subspace as

$$H_3^{\rm eff}(t) = \begin{bmatrix}
0 & 0 & g_1 & 0 & \Omega_1 \sin\theta \\
0 & 0 & g_1 & \Omega_2 \cos\theta e^{i\varphi_2} & 0 \\
g_1 & g_1 & 0 & 0 & 0 \\
0 & \Omega_2 \cos\theta e^{-i\varphi_2} & 0 & 0 & 0 \\
\Omega_1 \sin\theta & 0 & 0 & 0 & 0
\end{bmatrix}, \tag{24}$$

where we have set $\varphi_1 = 0$. A dark state exists for this system, since one eigenstate has eigenvalue 0:

$$\begin{aligned}
|D(t)\rangle = &\frac{\frac{g_1}{\Omega_1}\cos\theta}{\sqrt{\frac{g_1^2}{\Omega_1^2}\cos^2\theta + \frac{g_2^2}{\Omega_2^2}\sin^2\theta + \cos^2\theta\sin^2\theta}}|100\rangle\\
&+ \frac{e^{-i\varphi_2}\frac{g_2}{\Omega_2}\sin\theta}{\sqrt{\frac{g_1^2}{\Omega_1^2}\cos^2\theta + \frac{g_2^2}{\Omega_2^2}\sin^2\theta + \cos^2\theta\sin^2\theta}}|0\mathbf{a}_+0\rangle\\
&- \frac{\cos\theta\sin\theta}{\sqrt{\frac{g_1^2}{\Omega_1^2}\cos^2\theta + \frac{g_2^2}{\Omega_2^2}\sin^2\theta + \cos^2\theta\sin^2\theta}}|001\rangle.
\end{aligned} \tag{25}$$

Just like the case of the phase gate, if the system is initially prepared in the dark state, after a cycle of adiabatic evolution a pure geometric phase can be obtained. In this case, if the initial state is $|10\rangle_L$, we get a phase shift

$$\begin{aligned}
\phi_3 &= i\oint d\mathbf{R}\langle D(t)|\nabla_{\mathbf{R}}|D(t)\rangle\\
&= \oint d\varphi_2 \frac{\frac{g_2^2}{\Omega_2^2}\sin^2\theta}{\frac{g_2^2}{\Omega_2^2}\sin^2\theta + \frac{g_1^2}{\Omega_1^2}\cos^2\theta + \cos^2\theta\sin^2\theta}.
\end{aligned} \tag{26}$$

Note that this phase is not affected by the spatially inhomogeneous distribution of the cavity mode.

We also get a geometric phase for the subspace $\mathcal{H}^1 \otimes \mathcal{H}^2_-$. However, we can set choose our path to set this phase to 0 independently of ϕ_3. So, if we initially prepared the state $|10\rangle_L$ we get a geometric phase of ϕ_3 after the gate manipulations, and if the initial state is $|11\rangle_L$ the geometric phase is 0. The states $|00\rangle_L$ and $|01\rangle_L$ are not affected by this Hamiltonian, and hence also acquire no phase. The net effect is a two-qubit quantum gate,

$$\begin{aligned}
|00\rangle_L &\to |00\rangle_L,\\
|01\rangle_L &\to |01\rangle_L,\\
|10\rangle_L &\to e^{i\phi_3}|10\rangle_L,\\
|11\rangle_L &\to |11\rangle_L,
\end{aligned}$$

which is exactly the controlled phase gate we would like to implement.

As we can see in Eq. (25), the two clouds of atoms interact with each other by virtually absorbing and emitting a photon in cavity mode a, so leakage of cavity photons is the most important source of decoherence in our scheme. Analytically, the average photon number in the cavity during the process is

$$n_{\rm ph+} = \frac{\cos^2\theta\sin^2\theta}{\frac{g_1^2}{\Omega_1^2}\cos^2\theta + \frac{g_2^2}{\Omega_2^2}\sin^2\theta + \cos^2\theta\sin^2\theta}, \tag{27}$$

when the system is initially prepared in $|10\rangle_L$, and

$$n_{\rm ph-} = \frac{\cos^2\theta\sin^2\theta}{\frac{g_1^2}{\Omega_1^2}\cos^2\theta + \frac{g_3^2}{\Omega_3^2}\sin^2\theta + \cos^2\theta\sin^2\theta}, \tag{28}$$

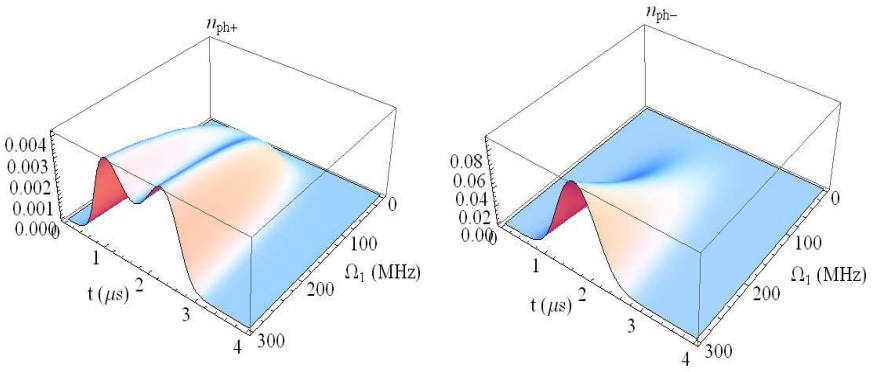

FIG. 11: (Color online.) The average number of photons in the cavity during gate operation as a function of time and Ω_1 for $g_1 = 660$MHz. (a) system initially prepared in $|10\rangle_L$ and (b) system initially prepared in $|11\rangle_L$.

when the system is initially prepared in $|11\rangle_L$, respectively. If the initial state is $|00\rangle_L$ or $|01\rangle_L$ there are no photons in the cavity.

Let's consider the concrete example of a conditional phase gate with $\phi_3 = \pi/16$. We set the parameters to be $g_+ = 20$MHz, $g_3 = g_- = 10$MHz, and the number of atoms in each cloud to be $N = 10^3$. Then we have $g_1 = 660$MHz, $\Omega_1 = 40$MHz, $\Omega_2 = 50$MHz and $\Omega_3 = 300$MHz. We choose

$$\theta(t) = \frac{\pi}{4}\exp[-(t-1.7)^2/0.5],$$

$$\varphi_2(t) = \frac{\pi}{4}\exp[-(t-2.115)^2/0.5],$$

(where time is expressed in μs). A numerical simulation (not including cavity loss) is shown in Fig. 10 where the initial state is $\frac{1}{4}|00\rangle_L + \frac{1}{4}|01\rangle_L + \frac{1}{4}|10\rangle_L + \frac{1}{4}|11\rangle_L$. The whole process is very fast and can be finished in 4μs, with extremely high accuracy approaching the theoretical value calculated in Eq. (26).

Fig. 11 shows the average number of cavity photons $n_{\rm ph+}$ and $n_{\rm ph-}$ during the process as a function of time and Ω_1 (not including cavity loss). The photon number is less than 0.001 in general, which means that the probability of a photon loss in the cavity is bounded above by 0.001 for the parameters given previously. We see that when the state of system is initially in $|11\rangle_L$, the average number of photons in the cavity is larger than in $|10\rangle_L$, $|00\rangle_L$ and $|01\rangle_L$. (Indeed, for the last two states the photon number is strictly zero.)

IV. MEASUREMENT

In fault-tolerant quantum computation, one must do syndrome measurement periodically [2, 42, 43], and the measurement results should be correct with high probability. It is also necessary to read out results at the end of a computation. Accurate measurement is therefore necessary. In this section, we propose a protocol to measure an atomic ensemble qubit in the computational basis.

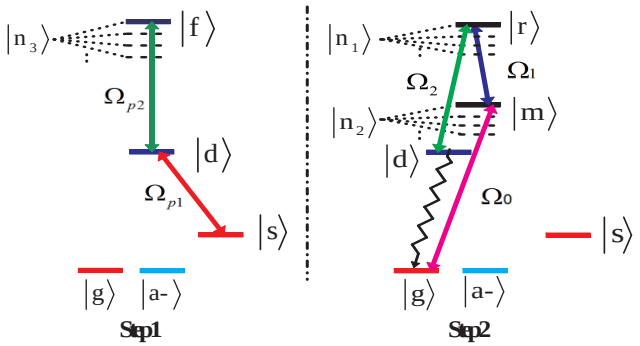

FIG. 12: (Color online.) The schematic setup to realize a projective measurement on a single qubit. Here, state $|d\rangle$ is a temporary state with a short lifetime. Transitions between $|d\rangle$ and $|s\rangle$ are not allowed. The state $|d\rangle$ can be chosen for example, to be $|F = 1, m_F = -1\rangle$ of the manifold $5P_{1/2}$.

Collecting the fluorescence from an atom is the most natural way to realize a measurement. For a single atom (or ion), many fluorescence photons are needed to make the measurement reliable, so a "cycling" transition from the computational state ($|0\rangle_L$ or $|1\rangle_L$) to an unstable excited state is generally used. In our case, however, there is an added complication. The computational states include superpositions of a single excitation over all the atoms of the cloud. The distance between atoms in the cloud can be several times larger than the wavelength of a photon emitted from the cloud, and this might make it possible (in principle) to distinguish which atom emitted the photon. This in turn could cause decoherence by collapsing the symmetric superposition, and take the system state outside the computational space. So we need a method to perform a reliable measurement while avoiding this problem.

As shown in Fig. 12, the procedure can be realized in

three steps:

1. Adiabatically transport the population of $|1\rangle_L$ to $|\mathbf{f}\rangle$. (The procedure is similar to that used in realizing the gate $R_y(\phi)$.)

2. Dynamically pump the atom cloud from the ground state to state $|\mathbf{m}\rangle$ with a π pulse Ω_0, and subsequently apply another π pulse Ω_1 between the state $|m\rangle$ and $|r\rangle$, finally, apply a third π pulse Ω_2 between state $|r\rangle$ and $|d\rangle$. Cycle this transition hundreds of times and collect the spontaneously emitted photons from the atom cloud.

3. Reverse step 1 to transfer the population of $|\mathbf{f}\rangle$ back to $|1\rangle_L$ to prepare for next operation.

If the qubit is initially in $|0\rangle_L$, step 1 has no effect. The state of the cloud will transfer to $|\mathbf{m}\rangle$ and then to $|\mathbf{r}\rangle$ and $|\mathbf{d}\rangle$ after three π pulses (the energy between $|r\rangle$ and $|d\rangle$ is the same as that of $|r\rangle$ and $|e\rangle$, therefore, no additional laser frequency is required for the measurement process.); the atom cloud will quickly decay to the ground state and emit a photon. By repeating this cycle many times, the probability of detecting the photons can be made quite high.

If the qubit is initially in $|1\rangle_L$, step 1 will produce a single excitation in $|f\rangle$, and by the dipole-dipole blockade effect the transition from the ground state to $|m\rangle$ will be blocked. Therefore we will not observe any emitted photons. Thus we observe fluorescence only if the qubit is initially in the state $|0\rangle_L$, and this procedure is a projective measurement. Note that non-uniform coupling is not a problem here since at the end of the procedure the state will be either $|0\rangle_L$ or $|1\rangle_L$.

The time for a single π laser pulse (and the accompanying state transition) should be roughly 10-20ns when Rabi frequency of the pumping laser is hundreds of MHz. Assuming a life time of about 10ns for $|d\rangle$, each cycle of measurement can be finished in 30-40ns. After the cycling transitions, we must transfer the population of $|\mathbf{f}\rangle$ back to $|1\rangle_L$, so we need the total measurement time to be less than the lifetime of $|f\rangle$ (estimated to be about 400μs). This gives an upper limit on the total number of cycles we can make during the process. If we want to limit the error to a reasonable level, we can perform at most a few hundred transition cycles. This should be adequate if the photodetector has sufficiently high efficiency and large enough solid angle of detection.

V. DECOHERENCE

A. Mechanisms

We will now consider the limitations imposed by decoherence on gate operation. For our system on atom chips to work, several main sources of noise have to be considered and kept under control, we treat them one at a time below. As a summary, Table I lists different decoherence channels, their mechanisms, their effects, and their typical rates on the atom chip system we are interested in.

1. Spontaneous Emission

Like all ion trap and neutral atom schemes in quantum computation, our proposal suffers from spontaneous emission when atoms are in excited states. In our scheme, the excited states (other than logical states) are never populated in the ideal case. However, in any real process (finite time, finite energy gap), the state of the system will precess around the dark state, instead of following it exactly in a perfect adiabatic way. This means that some population will reach the leaky excited states (including Rydberg states). We can calculate the population of such unwanted states during the adiabatic process and impose the condition:

$$\sum_k \int_0^T \gamma_k P_k(t) dt \ll 1, \tag{29}$$

where T is the duration of the gate, $P_k(t)$ is the population of the kth excited state of the atom, and γ_k is the corresponding decay rate of that state.

On the other hand, the condition for adiabatic process can be stated as:

$$\Omega_g T \gg 1. \tag{30}$$

Here, $E_g = \hbar\Omega_g$ estimates the difference between the dark state energy and the energy of the closest eigenstate. Suppose the kth excited state is an intermediate state used in our gate operation ($|e\rangle$ for the phase gate and the y-rotation gate, $|r_+\rangle$ or $|r_-\rangle$ for the controlled phase gate). We have $\max_t\{P_k(t)\} \approx 1/\Omega_g T$. Then the condition on γ_k must be:

$$\frac{\gamma_k T}{(\Omega_g T)^2} \ll 1. \tag{31}$$

2. Cavity Loss

Cavity loss may affect the controlled phase gate, which is realized based on the dark state in Eq. (25) through virtual emission and absorption of cavity photons. We note that even in the ideal adiabatic case, the state has nonzero projection onto the 1-photon cavity state, and so a lossy cavity will tend to destroy such a state. For the influence of the cavity loss rate to be small, the condition

$$\kappa \int_0^{T_{\rm cp}} \langle D(t)|a^\dagger a|D(t)\rangle dt \ll 1, \tag{32}$$

must be satisfied, where $\langle D(t)|a^\dagger a|D(t)\rangle$ is the population of the cavity mode during the adiabatic evolution, and $T_{\rm cp}$ is the duration of the controlled phase

gate. Since the integral above is always smaller than $\kappa T_{\rm cp}\max_t\{\langle D(t)|a^\dagger a|D(t)\rangle\}$, the inequality in our case can be replaced by

$$\kappa T_{\rm cp}\max_t\{n_{\text{ph-}}(t)\}=\kappa T_{\rm cp}\frac{\Omega_1^2\Omega_3^2}{4\left(g_1^2\Omega_3^2+g_3^2\Omega_1^2\right)}\ll 1. \quad (33)$$

Combined with Eq. (31), this inequality bounds the process time. Since our scheme has large g_1, it has a good ability to tolerate cavity loss, while still allowing a long process time to overcome the spontaneous emission for the controlled phase gate.

3. Trap Loss

It is crucial in our scheme to be able to store the atoms inside the trap as long as possible. However, there are several possible sources of noise to drive the atoms out of the trap, as shown in Ref. [23]. These noise sources can be divided into two groups:

1. Noise-induced spin-flip. Our logical states are encoded in two weak-field-seeking hyperfine states. If the state of an atom is flipped to the strong-field-seeking state, the magnetic potential is no longer a trap for that atom. Such spin-flips may be caused by fluctuations produced by thermally excited currents in the metallic substrate, or simply by technical noise in the wire currents.

2. Heating. The energy exchange increases both the system's mean energy and its energy spread, and can excite atoms to a high energy vibrational mode. Since the trap cannot be made infinitely deep, atoms may escape from the trap.

We assume that the loss rate is not too high when the temperature is low, and that the noise from substrate and wire currents is well controlled. If the system is in the ground state $|\mathbf{g}\rangle$, the loss of atoms will not cause decoherence at all. Only if the system is in a collective excited state does trap loss mean information is lost to the environment. For simplicity in the following discussion, we assume the loss rate of internal state $|k\rangle$ to be Γ_k. We see that loss of atoms is similar to spontaneous emission when the loss rate is low. Both effects can be treated as an amplitude damping channel. This observation will help us to analyze its effect by numerical simulation.

4. Stray Electric Fields

Stray electric fields are produced by the adsorbing of rubidium atom onto the substrate of the chip and mirrors of the cavity, and other uncontrollable mechanisms. In our case, we can treat such an electric field as a spatially random distributed field that causes extra detuning while there is optical coupling between different energy levels. To analyze this noise, we suppose the system we are interested in has Hamiltonian $H_{\rm sys}$, and that the total Hamiltonian including the stray electric fields can be written

$$H_{\rm tot}=H_{\rm sys}+\sum_i\left(\sum_k\Delta_{st}^k(x_i)|k\rangle\langle k|\right) \quad (34)$$

in the interaction picture. Here, $\Delta_{st}^k(x_i)$ is the extra detuning of the affected excited state $|k\rangle$ of atom i at position x_i relative to the center of the trap. Suppose the trap can be modeled as a harmonic oscillator. We have

$$x_i=\sqrt{\frac{1}{2m\nu}}(b_i+b_i^\dagger),$$

where ν is the frequency of the trap, and b_i ($b_i^\dagger$) is the lowering (raising) operator for atom i in the trap. Considering the limit where $\Delta_{st}^k(x_i)$ changes slowly and smoothly spatially near by the trap, we can expand it around the center of the trap:

$$\Delta_{st}^k(x_i)\approx\Delta_{st}^k(0)+\Delta_{st}^{k\prime}(0)x_i.$$

If the temperature is low enough, i.e, $kT\ll\hbar\nu$, most atom stay in the ground state, so b_i ($b_i^\dagger$) can be approximated as $b_i\approx|0\rangle_i\langle 1|$ ($b_i^\dagger\approx|1_i\rangle\langle 0_i|$), with $|0_i\rangle$ and $|1_i\rangle$ the ground state and first excited state of the atom i, respectively. Techniques similar to those in Section II can be applied here to put the Hamiltonian in the second quantizated representation:

$$H_{\rm tot}=H_{\rm sys}+\sum_k\left(\Delta_{st}^k(0)\hat{\mathcal{K}}^\dagger\hat{\mathcal{K}}+\tilde{\Delta}_{st}^{k\prime}(0)\hat{\mathcal{K}}^\dagger\hat{\mathcal{K}}(\hat{\mathcal{B}}^\dagger+\hat{\mathcal{B}})\right), \quad (35)$$

for some random numbers $\Delta_{st}^k(0)$ and $\tilde{\Delta}_{st}^{k\prime}(0)$ ($\Delta_{st}^{k\prime}(0)/\sqrt{2m\nu}$). Here, we define

$$\hat{\mathcal{K}}=\frac{1}{\sqrt{N}}\sum_i|g_i\rangle\langle k_i|$$

for different excited states $|k\rangle$, and

$$\hat{\mathcal{B}}=\frac{1}{\sqrt{N}}\sum_i|0_i\rangle\langle 1_i|.$$

Eq. (35) will be used in a numerical analysis of the effect of stray electric fields later.

B. Numerical Analysis

We performed numerical simulations of the universal set of quantum gates described in previous sections. These simulation confirm what we stated in the previous section. The robustness of gates against noise is measured by the fidelity of the gate, i [2]:

$$F_i=\min_{|\psi\rangle}\sqrt{\langle\psi|U_i^\dagger\mathcal{L}(|\psi\rangle\langle\psi|)U_i|\psi\rangle}, \quad (36)$$

Decoherence Channel	Mechanism	Effect	Typical Rate
Spontaneous emission		Excited states decay to ground state.	1kHz—100MHz
Cavity loss		Destroy the dark state through photon leakage.	10kHz—100MHz
Noise in the wire currents	Flip the spin state through fluctuation of magnetic potential.	Trap loss.	1Hz—1kHz
Thermally excited currents	Flip the spin state through fluctuation of magnetic potential.	Trap loss.	1Hz—1kHz
Heating	Excite atoms to high energy vibrational mode.	Trap loss.	1Hz—1kHz
Stray electrical field	Generate random phase.	Dephasing.	1MHz—1GHz

TABLE I: Decoherence mechanism for the atom chip system. Some of the typical values are based on [23] and [12].

where U_i is the desired gate operation and the superoperator $\mathcal{L}$ is determined by the master equation:

$$\frac{d}{dt}\rho = -i\left[H_{\rm sys},\rho\right] + \sum_j \left(L_j\rho L_j^\dagger - \frac{1}{2}L_j^\dagger L_j\rho - \frac{1}{2}\rho L_j^\dagger L_j\right) \equiv \mathcal{L}\rho, \tag{37}$$

in the Markov approximation. Here, the $\{L_j\}$ are the Lindblad operators representing the interaction with the environment. In many cases, no analytical solution of such master equation is known and even a numerical solution can be hard. We solve this equation by unraveling the density operator evolution into quantum trajectories [39]. The unraveling of the master equation implemented are given by the quantum state diffusion (QSD) equation [40] :

$$\begin{aligned}|d\psi\rangle =& -iH_{\rm tot}dt \\ &+ \sum_j \left(\langle L_j^\dagger\rangle_\psi L_j - \frac{1}{2}L_j^\dagger L_j - \frac{1}{2}\langle L_j^\dagger\rangle_\psi\langle L_j\rangle_\psi\right)|\psi\rangle dt \\ &+ \sum_j \left(L_j - \langle L_j^\dagger\rangle_\psi\right)|\psi\rangle d\xi_j.\end{aligned} \tag{38}$$

Here, angular brackets denote quantum expectations $\langle L_j\rangle_\psi = \langle\psi|L_j|\psi\rangle$, and $H_{\rm tot}$ is given by Eq. (35), which is a Hamiltonian with random parameters for each trajectory. The $d\xi_j$ are independent complex Gaussian differential random variables satisfying the conditions

$$\mathbb{E}[d\xi_j] = \mathbb{E}[d\xi_i d\xi_j] = 0, \text{ and } \mathbb{E}[d\xi_i^* d\xi_j] = \delta_{ij}dt,$$

where $\mathbb{E}$ denotes the ensemble mean. The density operator ρ is given by the mean over the projectors onto thee quantum states of the ensemble:

$$\rho = \mathbb{E}[|\psi\rangle\langle\psi|].$$

In this paper, we present fidelity calculations for the given set of universal gates, considering several channels of decoherence which are important in experiments. The simulation was realized with the "Quantum State Diffusion" C++ library [39] using a fourth-order Runge-Kutta integrator [41] and a pseudo random number generator to solve the master equation using quantum trajectories. For each trajectory, $\Delta_{st}^k(0)$ and $\tilde{\Delta}_{st}^{k\prime}(0)$ are Gaussian distributed random variables, i.e., $\Delta_{st}^k(0) \sim \mathcal{N}(\mu_k, \sigma_k^2)$ and $\tilde{\Delta}_{st}^{k\prime}(0) \sim \mathcal{N}(\mu_k', \sigma_k'^2)$.

1. *Phase Gate*

For the phase gate, spontaneous emission and trap loss, can affect the gate operation. The spontaneous emission rate γ_e from the state excited state $|e\rangle$ can destroy the superposition of hyperfine ground states when γ_e is large, though if we adiabatically transfer the state, the population of $|e\rangle$ is very small. As discussed in Ref. [11], the rate of spontaneous emission of the ensemble of atoms should be the same as of single atoms. The loss rates of atoms from the trap Γ_e, Γ_s, Γ_a for different energy level must also be included. As mentioned earlier, loss of atoms and spontaneous emission have the same effect so that they should share the same form of Lindblad operator. For simplicity of analysis, we conservatively set $\Gamma = \max(\Gamma_e, \Gamma_a)$, $\gamma = \gamma_e + \Gamma_e$, and choose the Lindblad operators to be: $L_1 = \sqrt{2\gamma}\hat{\mathcal{E}}$, $L_2 = \sqrt{2\Gamma}\hat{\mathcal{S}}$, and $L_3 = \sqrt{2\Gamma}\hat{\mathcal{A}}$.

We first simulate the case where there is no stray electric field. The simulation uses the initial state $|\psi\rangle = |1\rangle_L$, which minimize the fidelity. The result of the calculation is shown in Fig. 13 for different values of γ and Γ. (Each point is based on 100 trajectories, so this is not a highly precise calculation.) When Γ is in the range between 10Hz and 100Hz, the fidelity doesn't change dramatically and can be as high as 0.9999 when γ is less than 1MHz. Next, we consider the effect of noisy

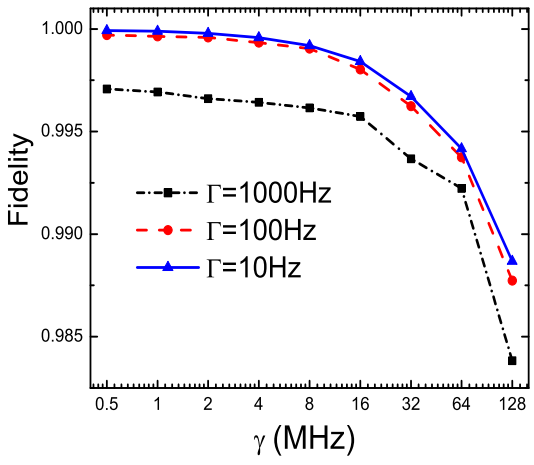

FIG. 13: (Color online.) Fidelity of a phase gate with $\phi_1 = \pi/8$ as a function of γ for different values of Γ not including stray fields.

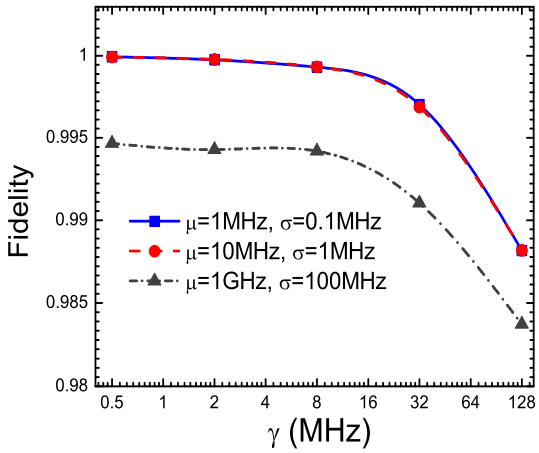

FIG. 14: (Color online.) Fidelity of a phase gate with $\phi_1 = \pi/8$ for different values of γ with $\Gamma = 10$Hz considering the stray field effect.

stray electric fields by solving Eq. (35) for state $|e\rangle$ with Δ^e_{st} and $\tilde{\Delta}^{e\prime}_{st}$. Again, for simplicity we conservatively assume $\mu = \max(\mu_e, \mu'_e)$ and $\sigma = \max(\sigma_e, \sigma'_e)$, with $\Delta^e_{st}(0) \sim \mathcal{N}(\mu, \sigma^2)$ and $\tilde{\Delta}^{e\prime}_{st}(0) \sim \mathcal{N}(\mu, \sigma^2)$. The simulation result shown in Fig. 14 is based on 100 trajectories for each point. The noisy electric field has almost no effect on the gate operation until it is about an order of magnitude larger than the Rabi-frequency Ω we applied on the atoms.

2. Y-Rotation Gate

For the y-rotation gate, we need to consider additional pumping processes as well as the adiabatic process to get the geometric phase. To simplify the calculation, we consider the fidelities defined in Eq. (36) for each process and multiply them together:

$$F = F_{p_1} \cdot F_{p_2} \cdot F_{p_1} \cdot F_{p_g} \cdot F_{p_2}, \tag{39}$$

where F_{p1} is fidelity of adiabatic transfer from state $|1\rangle_L$ to state $|\mathbf{f}\rangle$, F_{p_2} is the fidelity of the adiabatic pumping process from $|0\rangle_L$ to $|\mathbf{r}\rangle$, and F_{p_g} is the fidelity of the non-Abelian geometric process.

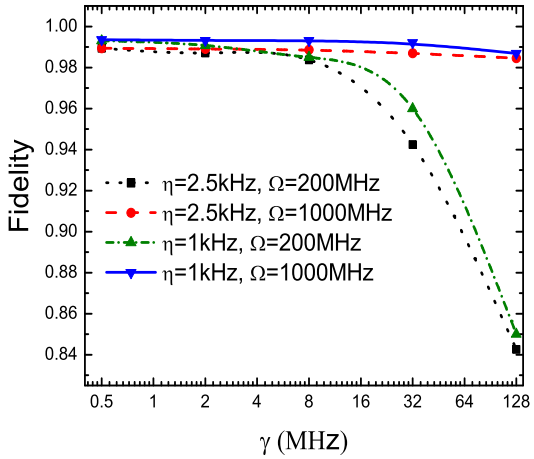

FIG. 15: (Color online.) Fidelity of a phase gate with $\phi_2 = \pi/4$ for different values of γ, η and Ω for $\Gamma = 100$Hz without considering the stray field.

According to Fig. 5, we need to consider both the loss from Rydberg states and from intermediate states. Just as for the phase gate, the parameters are chosen to be: $\Gamma = \max(\Gamma_e, \Gamma_{a_+}, \Gamma_s, \Gamma_m, \Gamma_r, \Gamma_f)$, $\gamma = \max(\gamma_e, \gamma_d)$, $\eta = \max(\gamma_m + \Gamma, \gamma_r + \Gamma, \gamma_f + \Gamma)$ and the Lindblad operators to be: $L_1 = \sqrt{2\eta}\hat{\mathcal{M}}, L_2 = \sqrt{2\eta}\hat{\mathcal{R}}, L_3 = \sqrt{2\eta}\hat{\mathcal{F}}, L_4 = \sqrt{2\gamma}\hat{\mathcal{E}}, L_5 = \sqrt{2\gamma}\hat{\mathcal{D}}, L_6 = \sqrt{2\Gamma}\hat{\mathcal{S}}$, and $L_7 = \sqrt{2\Gamma}\hat{\mathcal{A}}_+$ according to the corresponding loss channels. We first simulate the case where there is no additional noisy stray electric field. The simulation result is shown in Fig. 15 for $\Gamma = 100$Hz. The fidelity is beyond 0.99 when γ is less than 1MHz, η is 1kHz, and $\Omega = 1000$MHz. When γ is small, the error rate is dominated by η. When γ is high, the error rate is dominated by γ. The larger the Ω is, the smaller is the population of the intermediate state. Thus satisfying the condition (31) greatly reduces the error. The main reason why this gate can not achieve fidelity as high as 0.999 is due to the imperfect adiabatic pumping process p_2. However, our calculation is based on taking the minimum value of the dipole-dipole interaction over all pairs of atoms in the cloud, more accurate

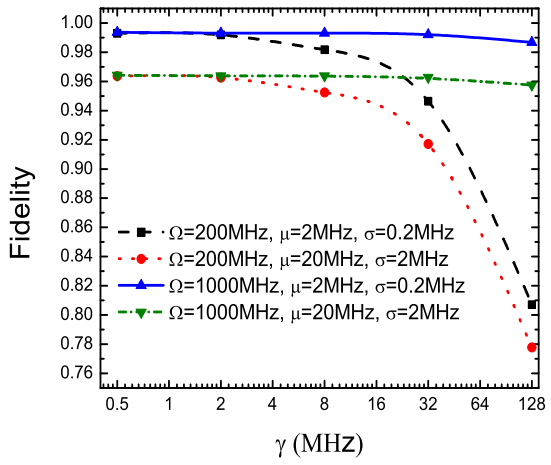

FIG. 16: (Color online.) Fidelity of a phase gate with $\phi_2 = \pi/4$ for different values of γ and Ω considering the stray field with $\eta = 1k$Hz and $\Gamma = 100$Hz.

simulation model of the dipole-dipole interaction would give better result.

In this case, the noisy stray field has different ways to affect our systems for different processes. According to Eq. (35), we have $|k_1\rangle = |d\rangle$ for process p_1, $|k_2\rangle = |m\rangle$ for process p_2, and $|k_3\rangle = |e\rangle$ for process p_g. The parameters are chosen to be $\mu = \max(\mu_e, \mu'_e, \mu_m, \mu'_m, \mu_d, \mu'_d)$ and $\sigma = \max(\sigma_e, \sigma'_e, \sigma_m, \sigma'_m, \sigma_d, \sigma'_d)$, with $\Delta^k_{st}(0) \sim \mathcal{N}(\mu, \sigma^2)$ and $\tilde{\Delta}^{k\prime}_{st}(0) \sim \mathcal{N}(\mu, \sigma^2)$ for $k = d, m, e$. The simulation results of the effect of noisy stray fields is shown in Fig. 16, with $\Gamma = 100$Hz, $\eta = 1$kHz and 100 trajectories for each point. The robust against the noisy electric field is not as good as the other two gates (we will see the case for the controlled-phase gate next) because of p_2. When the average amplitude of the noisy field is comparable to the amplitude of the Rabi frequency of the laser used in adiabatic pumping (which in this case, is 20MHz), some extra Raman transition-like processes will occur to excite the ensemble to higher excited states even though the strong dipole-dipole interaction between atoms forbids these excitations. If μ can be reduced as low as a few MHz, we can safely neglect the effect of noisy electric fields.

3. *Controlled Phase Gate*

For the controlled phase gate, besides the spontaneous emission and trap loss we analyzed for the single qubit gates, cavity loss also plays an important role. In our analysis, as shown in Fig. 9, the parameters are chosen conservatively to be: $\Gamma = \max(\Gamma_e, \Gamma_{a-}, \Gamma_{a+}, \Gamma_s)$, $\gamma = \max(\gamma_{r_-} + \Gamma_{r_-}, \gamma_{r_+} + \Gamma_{r_+})$ and we set the Lindblad operators to be $L_1 = \sqrt{2\gamma}(\hat{\mathcal{R}}_+)_1$, $L_2 = \sqrt{2\gamma}(\hat{\mathcal{R}}_+)_2$, $L_3 = \sqrt{2\Gamma}(\hat{\mathcal{S}})_1$, $L_4 = \sqrt{2\Gamma}(\hat{\mathcal{A}}_+)_2$, $L_5 = \sqrt{2\gamma}(\hat{\mathcal{S}}^\dagger)_1(\hat{\mathcal{R}}_+)_1$, $L_6 = \sqrt{2\Gamma}(\hat{\mathcal{S}}^\dagger)_2(\hat{\mathcal{A}}_+)_2$, $L_7 = \sqrt{2\gamma}(\hat{\mathcal{R}}_-)_2$, $L_8 = \sqrt{2\gamma}(\hat{\mathcal{S}}^\dagger)_2(\hat{\mathcal{R}}_-)_2$, $L_9 = \sqrt{2\gamma}(\hat{\mathcal{A}}^\dagger_-)_2(\hat{\mathcal{R}}_-)_2$, $L_{10} = \sqrt{2\Gamma}(\hat{\mathcal{S}})_2$, $L_{11} = \sqrt{2\Gamma}(\hat{\mathcal{A}}_-)_2$ and $L_{12} = \sqrt{2\kappa}a_{\rm cav}$ according to the corresponding channels.

We first simulate the case where there is only cavity loss. As stated previously, the initial state $|11\rangle_L$ emits more photons than the other three basis states during the gate operation. Hence, we take $|\psi\rangle = |11\rangle_L$ as the worst case.

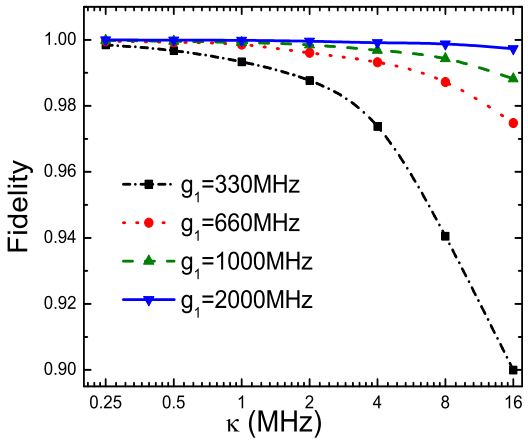

FIG. 17: (Color online.) Fidelity of the controlled phase gate with $\phi_3 = \pi/16$ for different values of κ and g_1 without any other decoherence channels included.

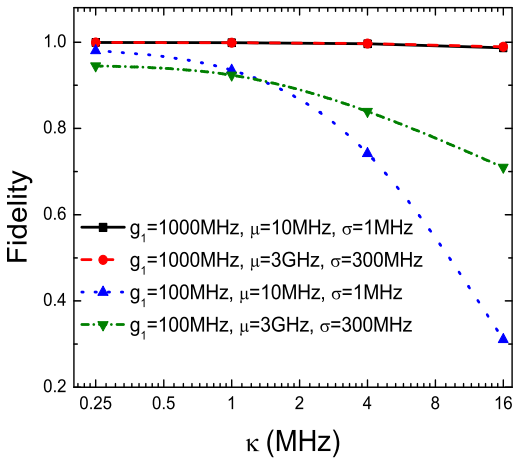

FIG. 18: (Color online.) Fidelity of the controlled phase gate with $\phi_3 = \pi/16$ for different values of κ and g_1 including the stray field effect, with $\Gamma = 100$Hz and $\gamma = 2.5$kHz.

The result of the numerical calculation in shown in Fig. 17, based on 100 trajectories for each point. From

Eq. (26), we see that ϕ_3 is approximately independent of g_1 and g_2 when they are large enough, so we can compare the fidelity for different value of g_1 for the same operation. Fig. 17 shows the gate fidelity for different values of κ and g_1. The larger the value of g_1 for this case, the easier condition (32) is to satisfy and the higher fidelity we get. The fidelity can exceed 0.9999 when κ is less than 500kHz for $g_1 = 2000$MHz, and exceed 0.999 when κ is less than 500kHz for $g_1 = 660$MHz, and when κ is less than 1MHz for $g_1 = 1000$MHz. For a FP cavity larger than 100μm, values of κ under 1MHz are quite achievable, and even for large values of κ, the fidelity is still acceptable for some schemes of fault tolerant quantum computation. When $g_1 = 330$MHz, the performance is bad for large value of κ.

Finally, we analyze the stray electric field effect on $|r_-\rangle$ ($|r_+\rangle$) with $\Delta_{st}^{r_-}$ ($\Delta_{st}^{r_+}$) and $\tilde{\Delta}_{st}^{r_-\prime}$ ($\tilde{\Delta}_{st}^{r_+\prime}$). The simulation result in shown in Fig. 18 with $\Gamma = 100$Hz and $\gamma = 2.5$kHz. It's worth noting that the random electric field does not affect the gate operation until it is an order of magnitude larger than the effective cavity coupling strength g_1. For a smaller value of g_1, such as 100MHz here, when κ is large, the photon no longer be able to stay in the cavity for long enough to do the gate operation, In that regime the gate construction breaks down. However, when large stray fields exist in that regime, the detuning they induce further reduces the number of photons in the cavity, and give an even better fidelity.

VI. CONCLUSIONS

In this paper we have proposed a scheme to achieve quantum computation using geometric manipulation of ensembles of atoms in a cavity QED system. Adiabatic optical control can be used to obtain a geometric phase gate and controlled phase gate. Combining optical excitation with a dipole-dipole blockade between Rydberg states allows us to geometrically realize the $R_y(\phi_2)$ gate. Thus a universal set of quantum gates can be realized geometrically.

We analyzed this scheme for ensembles of neutral rubidium atoms, magnetically trapped in planoconcave microcavities on an atom chip. Numerical simulations show that a single qubit gate can be performed in several microseconds with very low probability of gate error if the Rabi-frequency of coupling laser is larger than the average amplitude of stray electric fields and the rate of spontaneous emission. For the controlled phase gate, the operation is done by virtually emitting and absorbing a photon from the cavity mode, and can be completed in one single step operation, in a short time (about 4μs) for a controlled $\pi/32$, gate with very high fidelity even in a noisy environment thanks to the strong effective coupling efficiency between cavity photon and atoms. An advantage of geometric manipulation is that by adiabatic parameter control, we can avoid certain kinds of errors, especially those caused by inhomogeneous distribution of the laser beam and cavity modes. The values of the fields can depend on atom position, but their ratio can be fixed and controllable. The basic idea is to find an appropriate adiabatic process, so that the relevant dynamics are either independent of, or depend only on the ratio of, the two coupling rates.

The ensemble of atoms effectively enlarges the coupling rate g by $\sqrt{N}$, which greatly suppresses the likelihood of cavity photons and increases the fidelity of the operation. We analyzed the scheme for $N = 10^3$ atoms in each cloud. The parameters that we have assumed in our numerical simulations are all achievable by current experiments. This, together with the possibility of coupling stationary qubits (for computation) with flying qubits (for communication) makes this scheme look particularly promising for near-term quantum protocols.

ACKNOWLEDGMENTS

TAB and YZ acknowledge support from NSF Grants EMT-0829870 and CCF-0448658.

APPENDIX

In this appendix, we discuss how to choose appropriate Stark eigenstates of alkali atoms for our purpose. Since alkali atoms have spectra similar to hydrogen, we first analyze the effect of the dipole-dipole interaction on Rydberg stark eigenstates for hydrogen. After that, we allow for the difference between alkali atoms and hydrogen, and discuss a method of calculating their energy structure. Using this method, we will choose appropriate Rydberg Stark eigenstates of rubidium as an example. (Please note that the fine structure of the p and d states of rubidium have observable effects on the spectrum. However, for simplicity, we do not take this into account.) The method of calculation is described in detail in Ref. [44]. Note that all quantities below are in atomic units for simplicity.

We first consider Stark states of a single hydrogen atom. The magnetic quantum number m is a good quantum number. From perturbation theory, the first order approximation of Stark eignstates are parabolic states $|n, n_1, n_2, m\rangle$ [44] with energies

$$E_{n,n_1,n_2,m} = -\frac{1}{2n^2} + \frac{3}{2}E(n_1 - n_2)n.$$

Here, n is the principal quantum number, E is the electric field in the z direction, and n_1, n_2 are non-negative integers satisfying the equality $n = n_1 + n_2 + |m| + 1$. For $m = 0$, allowed values of $n_1 - n_2$ are $n-1, n-3, ..., -n+1$ and for $m = 1$, they are $n-2, n-4, ..., -n+2$. In the following discussion, we use the quantum number $q = n_1 - n_2$ instead of n_1 and n_2 for simplicity.

We expand the Stark parabolic states $|n,m,q\rangle$ in the spherical basis $|n,l,m\rangle$ as [44]:

$$|n,m,q\rangle = \sum_{l=0}^{n-1} |n,l,m\rangle\langle n,l,m|n,m,q\rangle. \tag{40}$$

The coefficients can be written in terms of Wigner 3J symbols [44]:

$$\begin{aligned} c(n,l,m,q) \equiv &\langle n,l,m|n,m,q\rangle = (-1)^{(1-n+m+q)/2+l} \\ &\times \sqrt{2l+1} \begin{pmatrix} \frac{n-1}{2} & \frac{n-1}{2} & l \\ \frac{m+q}{2} & \frac{m-q}{2} & -m \end{pmatrix}. \end{aligned} \tag{41}$$

For example, if $n=2$, $m=0$, $q=1$, we have $c(2,0,0,1) = \sqrt{2}/2$ and $c(2,1,0,1) = -\sqrt{2}/2$. So, $|2,0,1\rangle = (\sqrt{2}/2)|2,0,0\rangle - (\sqrt{2}/2)|2,1,0\rangle$. We will frequently use these parabolic states instead of spherical states in the following analysis.

The dipole-dipole interaction $V_{\rm dip}$ is proportional to $\widehat{\mathbf{r}}_1 \cdot \widehat{\mathbf{r}}_2$, where

$$\widehat{\mathbf{r}}_1 = r_1(\frac{x_1}{r_1}\mathbf{e}_x + \frac{y_1}{r_1}\mathbf{e}_y + \frac{y_1}{r_1}\mathbf{e}_z) \otimes I,$$

$$\widehat{\mathbf{r}}_2 = I \otimes r_2(\frac{x_2}{r_2}\mathbf{e}_x + \frac{y_2}{r_2}\mathbf{e}_y + \frac{y_2}{r_2}\mathbf{e}_z),$$

are coordinate operators for atoms 1 and atom 2. Replacing x, y, z with spherical coordinates r, θ, ϕ,

$$\begin{aligned} x &= r\sin\theta\cos\phi, \\ y &= r\sin\theta\sin\phi, \\ z &= r\cos\theta. \end{aligned} \tag{42}$$

gives us

$$\begin{aligned} &V_{\rm dip} \propto \widehat{\mathbf{r}}_1 \cdot \widehat{\mathbf{r}}_2 \\ =&r_1(\frac{x_1}{r_1}\mathbf{e}_x + \frac{y_1}{r_1}\mathbf{e}_y + \frac{y_1}{r_1}\mathbf{e}_z) \cdot r_2(\frac{x_2}{r_2}\mathbf{e}_x + \frac{y_2}{r_2}\mathbf{e}_y + \frac{y_2}{r_2}\mathbf{e}_z) \\ =&r_1\sqrt{\frac{4\pi}{3}}(\frac{\mathbf{e}_x + i\mathbf{e}_y}{\sqrt{2}}Y^1_{1,-1} + \frac{i\mathbf{e}_y - \mathbf{e}_x}{\sqrt{2}}Y^1_{1,1} + Y^1_{1,0}\mathbf{e}_z)\cdot \\ &r_2\sqrt{\frac{4\pi}{3}}(\frac{\mathbf{e}_x + i\mathbf{e}_y}{\sqrt{2}}Y^2_{1,-1} + \frac{i\mathbf{e}_y - \mathbf{e}_x}{\sqrt{2}}Y^2_{1,1} + Y^2_{1,0}\mathbf{e}_z) \\ =&\frac{4\pi}{3}r_1r_2(-Y^1_{1,-1}Y^2_{1,1} - Y^1_{1,1}Y^2_{1,-1} + Y^1_{1,0}Y^2_{1,0}), \end{aligned} \tag{43}$$

where $Y^i_{l,m}$ is a spherical harmonic function for atom i. Generally speaking, for two atoms in the given initial Stark eigenstate, the diagonal terms of the dipole-dipole interaction give an energy shift, while its non-diagonal terms couple adjacent m manifolds with each other: (m,m) to $(m\pm1, m\mp1)$. The Stark states that are most useful for our scheme are those that maximize the energy shift while suppressing the transition between different m manifolds (which might introduce decoherence channels). So it is sufficient for us to know the value of the matrix elements

$$\begin{aligned} &\langle n,m|\langle n,m,q|V_{\rm dip}|n',m+1\rangle|n',m-1\rangle, \\ &\langle n,m|\langle n,m,q|V_{\rm dip}|n',m-1\rangle|n',m+1\rangle, \end{aligned} \tag{44}$$

and

$$\langle n,m,q|\langle n,m,q|V_{\rm dip}|n',m,q\rangle|n',m,q\rangle. \tag{45}$$

For hydrogen, we will only consider matrix elements with the same n for simplicity. Even so, it is too complicated (and unnecessary) to find the general analytical form of these elements. Instead, we numerically do the integration to determine which states fulfill our requirements. By symmetry, the transition strengths of $(m,m) \to (m+1,m-1)$ and $(m,m) \to (m-1,m+1)$ are the same, so we just give the first value. The calculation results for some matrix elements are shown in Table II as an example.

We have made several simplifications in this table. First, we didn't calculate the transition strengths between different n manifolds, because they are several times smaller than their counterparts in the same n manifold. Second, we didn't calculate the case when two atoms are initially prepared in different Stark eigenstates, especially in two different manifolds, which actually we *have* proposed to realize both the gate $e^{\phi_2\sigma_y}$ and qubit measurement. Nevertheless, this table gives enough information about the characteristics of the state we are looking for. First, the transition strength must be much smaller than the energy shift inside the same n manifold. Second, those transitions between initial and final states with a difference in parabolic number q larger than one must be greatly suppressed. If we prepare an atom in the outermost state $|n,m=0,q=n-1\rangle$, we obtain the largest energy shift with the smallest transition strength to the $(m+1,m-1)$ state compared with other Stark eigenstates in the same manifold.

In our proposed gate, since the Rydberg states of two atoms may not be in the same manifold, a natural solution to fulfill our requirements is to choose the state $|\Psi\rangle = |n,m=0,q=n-1\rangle|n',m=0,q=n'-1\rangle$ for manifolds n and n'. Note that the energy shift term in the Hamiltonian is a product of operators on two different atoms, so the analysis of two atoms in same manifold can be directly applied to show that the maximum energy shift is obtained if the two atoms are prepared in the state $|\Psi\rangle$. This gives an energy shift of

$$\langle\Psi|V_{\rm dip}|\Psi\rangle \propto n(n-1)n'(n'-1).$$

Next, we consider the case of non-hydrogen alkali atoms. Physically, the main difference between alkali atoms and hydrogen atoms is that the former have a finite sized ionic core that results in avoided crossings in the Stark spectrum. So, the Hamiltonian can be written as

$$H = -\frac{\nabla^2}{2} - \frac{1}{r} + V_d(r) + Ez. \tag{46}$$

Matrix element: $\|m,q\rangle \to \|m',q'\rangle$	n =5	n = 10	n = 15	n = 20	n = 25
$\|0,n-1\rangle\|0,n-1\rangle \to \|1,n-2\rangle\|-1,n-2\rangle$	112.5	1012.5	3543.75	8550	16875
$\|0,n-1\rangle\|0,n-1\rangle \to \|0,n-1\rangle\|0,n-1\rangle$	900	18225	99225	324900	810000
$\|0,n-1\rangle\|0,n-1\rangle \to \|1,n-4\rangle\|-1,n-4\rangle$	0	0	0	0	0
$\|0,n-3\rangle\|0,n-3\rangle \to \|1,n-2\rangle\|-1,n-4\rangle$	137.78	1350	4829.32	11769	23362.4
$\|0,n-3\rangle\|0,n-3\rangle \to \|1,n-4\rangle\|-1,n-2\rangle$	137.78	1350	4829.32	11769	23362.4
$\|0,n-3\rangle\|0,n-3\rangle \to \|1,n-4\rangle\|-1,n-4\rangle$	168.75	1800	6581.25	16200	32343.7
$\|0,n-3\rangle\|0,n-3\rangle \to \|1,n-2\rangle\|-1,n-2\rangle$	112.5	1012.5	3543.75	8550	16875
$\|0,n-3\rangle\|0,n-3\rangle \to \|0,n-3\rangle\|0,n-3\rangle$	225.01	11025	72900	260100	680625
$\|1,n-2\rangle\|1,n-2\rangle \to \|2,n-3\rangle\|0,n-3\rangle$	137.78	1350	4829.32	11769	23362.4
$\|1,n-2\rangle\|1,n-2\rangle \to \|1,n-2\rangle\|1,n-2\rangle$	506.25	14400	85556	291600	743906
$\|1,n-4\rangle\|1,n-4\rangle \to \|2,n-3\rangle\|0,n-5\rangle$	137.78	1350	4829.32	11769	23362.4
$\|1,n-4\rangle\|1,n-4\rangle \to \|2,n-5\rangle\|0,n-3\rangle$	168.75	2062.16	7744.14	19281.9	38742.1
$\|1,n-4\rangle\|1,n-4\rangle \to \|2,n-5\rangle\|0,n-5\rangle$	168.75	2062.16	7744.14	19281.9	38742.1
$\|1,n-4\rangle\|1,n-4\rangle \to \|2,n-3\rangle\|0,n-3\rangle$	137.78	1350	4829.32	11769	23362.4
$\|1,n-4\rangle\|1,n-4\rangle \to \|1,n-4\rangle\|1,n-4\rangle$	56.25	8100	61256.3	230400	620156

TABLE II: The matrix element of operator $V_{\rm dip}$ in atomic units.

Here, $V_d(r)$ is the difference of the potential function between a hydrogen and an alkali atom, due to the finite-sized ionic core. We treat $V_d(r)$ as spherically symmetric and only nonzero near the nucleus. In the case where quantum defects are relatively small (e.g., n is large), we can use the hydrogenic parabolic states as our working basis. For diagonal terms of the Hamiltonian, we have:

$$\begin{aligned}\langle n,m,q|H|n,m,q\rangle &= -\frac{1}{2n^2}+\frac{3}{2}qnE \\ &+ \langle n,m,q|V_d(r)|n,m,q\rangle + O(E^2),\end{aligned} \tag{47}$$

and we represent the non-diagonal terms using hydrogen spherical states $|n,l,m\rangle$:

$$\begin{aligned}\langle n,m,q|H|n',m,q'\rangle &= \sum_{l,l'}^{n-1}\langle n,m,q|n,l,m\rangle \\ &\times \langle n,l,m|V_d(r)|n',l',m\rangle\langle n',l',m|n',m,q'\rangle.\end{aligned} \tag{48}$$

Denote the spherically symmetric eigenstates of the alkali atom as $|n,l,m\rangle_{al}$. For large n, we have

$$\begin{aligned}-\frac{1}{2(n-\delta_l)^2} =& {}_{al}\langle n,l,m|H|n,l,m\rangle_{al} \\ \approx& \langle n,l,m|\left(-\frac{\nabla^2}{2}-\frac{1}{r}+V_d(r)\right)|n,l,m\rangle \\ =& -\frac{1}{2n^2}+\langle n,l,m|V_d(r)|n,l,m\rangle.\end{aligned} \tag{49}$$

where δ_l is the quantum defect for angular momentum l of the alkali atom [45], which is different for each element. For rubidium, if we neglect neglect the fine structure effect, $\delta_0 \approx 3.1$, $\delta_1 \approx 2.6$, $\delta_2 \approx 1.3$, and $\delta_3 \approx 0.02$. For $l > 3$, $\delta_l \approx 0$. On the other hand,

$$-\frac{1}{2(n-\delta_l)^2} \approx -\frac{1}{2n^2}-\frac{\delta_l}{n^3}.$$

So we have:

$$\langle n,l,m|V_d(r)|n,l,m\rangle \approx -\frac{\delta_l}{n^3}. \tag{50}$$

Per Ref. [44], this expression may be generalized to

$$\langle n,l,m|V_d(r)|n',l,m\rangle = -\frac{\delta_l}{\sqrt{n^3n'^3}}. \tag{51}$$

Here, we take advantage of the spherical symmetry of $V_d(r)$, so the matrix element vanishes when the l value on the two sides of the above equation are not the same.

Observe that Eq. (45) can be represented as matrix multiplication. We define matrices

$$\begin{aligned}[\mathcal{C}^{nm}]_{ql} =& \langle n,m,q|n,l,m\rangle = c(n,l,m,q), \\ [\mathcal{V}^{nm}]_{lq} =& \langle n,l,m|n,m,q\rangle = c(n,l,m,q), \\ [\mathcal{D}^{nn'}]_{ll'} =& \langle n,l,m|V_d(r)|n',l',m\rangle, \\ [\mathcal{S}^{nn'm}]_{qq'} =& \langle n,m,q|H|n',m,q'\rangle.\end{aligned} \tag{52}$$

Then, we have

$$\mathcal{S}^{nn'm} = \mathcal{C}^{nm}\mathcal{D}^{nn'}\mathcal{V}^{n'm}. \tag{53}$$

Note that these superscripts label a family of matrics, not matrix element indices. For the purpose of illustration, we show a simple example. We write the matrices

$$\mathcal{C}^{20} = \begin{bmatrix} \frac{1}{\sqrt{2}} & \frac{1}{\sqrt{2}} \\ \frac{1}{\sqrt{2}} & -\frac{1}{\sqrt{2}} \end{bmatrix},$$

$$\mathcal{V}^{30} = \begin{bmatrix} \frac{1}{\sqrt{3}} & \frac{1}{\sqrt{3}} & \frac{1}{\sqrt{3}} \\ \frac{1}{\sqrt{2}} & 0 & -\frac{1}{\sqrt{2}} \\ \frac{1}{\sqrt{6}} & -\sqrt{\frac{2}{3}} & \frac{1}{\sqrt{6}} \end{bmatrix},$$

$$\mathcal{D}^{23} = \begin{bmatrix} -\frac{\delta_0}{6\sqrt{6}} & 0 & 0 \\ 0 & -\frac{\delta_1}{6\sqrt{6}} & 0 \end{bmatrix},$$

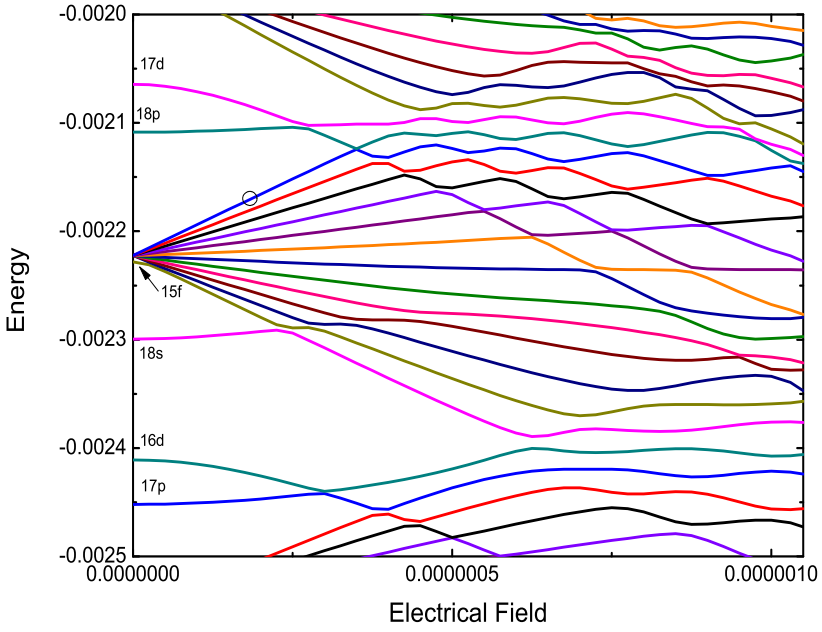

FIG. 19: (Color online.) The energy level of rubidium around manifold $n = 15$, $m = 0$. The circled states is our candidate states which have large energy shift.

and multiply them to get

$$\mathcal{S}^{230} = \begin{bmatrix} -\frac{\delta_0}{36} - \frac{\delta_1}{12\sqrt{6}} & -\frac{\delta_0}{36} & -\frac{\delta_0}{36} + \frac{\delta_1}{12\sqrt{6}} \\ -\frac{\delta_0}{36} + \frac{\delta_1}{12\sqrt{6}} & -\frac{\delta_0}{36} & -\frac{\delta_0}{36} - \frac{\delta_1}{12\sqrt{6}} \end{bmatrix}.$$

Matrix $\mathcal{S}^{nn'm}$ can be treated as a submatrix (or block) of the Hamiltonian matrix. Since the Hilbert space is infinite-dimensional, we need to truncate the Hamiltonian matrix. For example, if we need to know eigenvalues and eigenstates of manifold n of rubidium, we need to consider only those manifolds that couple to it.

We now calculate the energy structure of the $n = 15$ manifold for purposes of illustration. We also need to consider the adjacent manifolds such as $n = 14$, $n = 16$, $n = 17$ and $n = 18$, since states like 16d, 17p, 17d, 18s and 18p are coupled to the $n = 15$ manifold. Define the submatrix of the Hamiltonian $\mathcal{H}^{nn'm}$ as

$$[\mathcal{H}^{nn'm}]_{qq'} = [\mathcal{S}^{nn'm}]_{qq'} - \delta_{nn'}\delta_{qq'}(\frac{1}{2n^2} - \frac{3}{2}qnE),$$

where δ_{nm} is the Kronecker delta. The Hamiltonian matrix is approximately represented as:

$$\begin{bmatrix} \mathcal{H}^{14,14,m} & \mathcal{H}^{14,15,m} & \mathcal{H}^{14,16,m} & \mathcal{H}^{14,17,m} & \mathcal{H}^{14,18,m} \\ \mathcal{H}^{15,14,m} & \mathcal{H}^{15,15,m} & \mathcal{H}^{15,16,m} & \mathcal{H}^{15,17,m} & \mathcal{H}^{15,18,m} \\ \mathcal{H}^{16,14,m} & \mathcal{H}^{16,15,m} & \mathcal{H}^{16,16,m} & \mathcal{H}^{16,17,m} & \mathcal{H}^{16,18,m} \\ \mathcal{H}^{17,14,m} & \mathcal{H}^{17,15,m} & \mathcal{H}^{17,16,m} & \mathcal{H}^{17,17,m} & \mathcal{H}^{17,18,m} \\ \mathcal{H}^{18,14,m} & \mathcal{H}^{18,15,m} & \mathcal{H}^{18,16,m} & \mathcal{H}^{18,17,m} & \mathcal{H}^{18,18,m} \end{bmatrix}, \quad (54)$$

which is an 80×80 Hermitian matrix. Similar methods could be applied to much higher excitation states, like $n = 80$, that might be more suitable in practice.

By diagonalizing the Hamiltonian matrix, we can obtain the spectrum and the eigenstates. As mentioned earlier, the state we use should have a large component of $|n, m = 0, q = n-1\rangle$, which means we want the single-atom eigenstate

$$|r\rangle_{n,m} = \sum_q C_q |n, m, q\rangle$$

to have $m = 0$ with a large coefficient $|C_q|$ for $q = n - 1$.

Fig. 19 shows the spectrum around the manifold $n = 15$. The outermost Stark eigenstates $|r\rangle_{15,0}$, circled in the figure in the regime where the Stark eigenvalues are roughly linear in the electric field ($E \leq 2.5 \times 10^{-7}$), are good candidate states, since they should have behavior similar to the hydrogen state $|n, m = 0, q = n - 1\rangle$. Numerical calculation shows that the diagonal term of the dipole-dipole interaction is about 8×10^4 in $|r\rangle_{15,0}|r\rangle_{15,0}$ (compared to 99225 for hydrogen in the previous table), which is larger than for the other states in the manifold.

To put this in the context of our scheme for quantum computation, consider the case where there are 10^3 atoms in a volume of $(6\mu\text{m})^3$. The smallest energy shift of a pair of atoms inside the cell is for those that are most distant. Suppose the two most distant atoms are in the state $|r\rangle_{15,0}|r\rangle_{15,0}$. The energy shift between them should

be around 1MHz, depending on the spatial distribution of atoms. In our scheme, where two atoms may also be in different single-atom states (actually in different manifolds), we could naturally extend our original analysis, but we expect a similar result.

In practice, we would want to use higher energy Rydberg states; for instance an $n = 60$ state $|m\rangle = |r\rangle_{60,0}$ for the intermediate state and an $n = 70$ state $|r\rangle = |r\rangle_{70,0}$ for the register state, to get both longer lifetimes (more than 300-400μs for $n = 70$ can be achieved in a cryogenic environment [35]) and a stronger dipole-dipole interaction. Since higher energy Rydberg states should behave more like the Rydberg states of hydrogen, we can pick the outermost Stark eigenstates in the linear Stark area for both atoms, whether or not they have the same principal quantum number. If the initial state of one atom is in the outermost state of manifold $n = 60$, and the other in either manifold $n = 60$ or $n = 70$, then by $V_{\rm dip} \propto n(n-1)n'(n'-1)$ the energy shift should be roughly 200-300MHz or 300-400MHz, respectively. The distance of the most closely-spaced pair of atoms should be about $10^4 a_0$. This is larger than $2R$, where $R = 4900a_0$ is the radius of atoms in manifold $n = 70$. This spacing should satisfy the assumption of our dipole-dipole interaction model.

[1] D. P. Divincenzo, Science **270**, 255 (1995); C. H. Bennett, Phys. Today **48**(10), 24 (1995); C. H. Bennett and D. P. Divincenzo, Nature (London) **404**, 247 (2000).

[2] M. A. Nielsen and I. L. Chuang , *Quantum Computation and Quantum Information*, (Cambridge University Press, Cambridge 2000).

[3] G. Chen *et al.*, *Quantum Computing Devices: Principles, Devices, and Analysis*, (Chapman & Hall/CRC, 2006).

[4] J. I. Cirac and P. Zoller, Phys. Rev. Lett. **74**, 4091 (1995).

[5] A. Sørensen, K. Mølmer, Phys. Rev. Lett. **82**, 1971 (1999).

[6] G. K. Brennen *et al.*, Phys. Rev. Lett. **82**, 1060 (1999).

[7] D. Jaksch *et al.*, Phys. Rev. Lett. **85**, 2208 (2000).

[8] T. Pellizzari, S. A. Gardiner, J. I. Cirac and P. Zoller, Phys. Rev. Lett. **75**, 3788 (1995).

[9] S.-B. Zheng, G.-C. Guo, Phys. Rev. Lett. **85**, 2392 (2000).

[10] E. Knill, R. Laflamme, G. J. Milburn, Nature **409**, 46 (2001).

[11] M. D. Lukin, Rev. Mod. Phys. **75**, 457 (2003);

[12] M. Fleischhauer, A. Imamoğlu, and J. P. Marangos, Rev. Mod. Phys. **77**, 633 (2005).

[13] U. Schnorrberger *et al.*, Phys. Rev. Lett. **103**, 033003 (2009)

[14] M. D. Lukin *et al.*, Phys. Rev. Lett. **87**, 037901 (2001).

[15] A. V. Gorshkov, J. Otterbach, M. Fleischhauer, T. Pohl, M. D. Lukin, arXiv:1103.3700.

[16] M. Müller, I. Lesanovsky, H. Weimer, H. P. Büchler, and P. Zoller, Phys. Rev. Lett. **102**, 170502 (2009).

[17] H. Weimer, M. Müller, I. Lesanovsky, P. Zoller, H. P. Büchler, Nature. Phys. **6**, 382 (2010).

[18] A. Gaëtan. *et al.*, Nature. Phys. **5**, 115 (2009).

[19] E. Urban *et al.*, Nature. Phys. **5**, 110 (2009).

[20] D. Petrosyan, M. Fleischhauer, Phys. Rev. Lett. **100**, 170501 (2008).

[21] L.-M. Duan, J. I. Cirac, P. Zoller, Science **292**, 1695 (2001).

[22] A. Recati, T. Calarco, P. Zanardi, J. I. Cirac, P. Zoller, Phys. Rev. A. **66**, 13 (2002).

[23] R. Folman, P. Krüger, J. Schmiedmayer, J. Denschlag, and C. Henkel, Adv. Atom. Mol. Phy. **48**, 263 (2002)

[24] J. Fortágh and C. Zimmermann, Rev. Mod. Phys. **79**, 235 (2007).

[25] M. Trupke, J. Metz, A. Beige, E. A. Hinds, J. Mod. Opt. **54**, 1639 (2007).

[26] M. Trupke *et al.*, Appl. Phys. Lett. **87**, 211106 (2005).

[27] E. Charron *et al.*, Phys. Rev. A **74**, 012308 (2006).

[28] P. Treutlein *et al.*, Phys. Rev. Lett. **92** 203005 (2004).

[29] M. Fleishhauer, S. F. Yelin, M. D. Lukin, Opt. Comm. **179**, 395 (2000).

[30] M. D. Lukin, S. F. Yelin, M. Fleischhauer, Phys. Rev. Lett. **84**, 4232 (2000).

[31] P. Zanardi, M. Rasseti, Phys. Lett. A **264**, 94 (1999).

[32] M. V. Berry, Proc. R. Soc. London A. **392**, 45 (1984).

[33] F. Wilczek, A. Zee, Phys. Rev. Lett. **52**, 2111 (1984).

[34] S. Lloyd, Phys. Rev. Lett. **75**, 346 (1995).

[35] M. Saffman and T. G. Walker, Phys. Rev. A **72**, 022347 (2005).

[36] J. Simon *et al.*, Nature.Phys. **3**, 765 (2007)

[37] L.-M. Duan, A. Kuzimich, H. J. Kimble, Phys. Rev. A. **67**, 032305 (2003).

[38] D. F. Walls and G. J. Milburn, *Quantum Optics* (Springer-Verlag, 1994).

[39] R. Shack and T. A. Brun, Comp. Phys. Comm. **102**, 210 (1997).

[40] N. Gisin and I. C. Percival, J. Phys. A **25**, 5677 (1992).

[41] W. H. Press *et al.*, *Numerical Recipes in C* (Cambridge University Press, 2002).

[42] D. Gottesman, Ph.D. thesis, Caltech, 1997.

[43] D. Gottesman, Phys. Rev. A **57**, 127 (1998).

[44] T. F. Gallagher, *Rydberg Atoms* (Cambridge University Press, 1994).

[45] C. J. Foot, *Atomic Physics* (Oxford University Press, 2005).